A Hedgehog-Induced Homeodomain Cascade Couples Progenitor Identity to Neuronal Diversification

Chundi Xu*[1], Rishi G. Sastry[1], Peter Newstein[1], Ryan N. Delgado[2], Neel Wagh[3], Marion Silies[3], Constance L. Cepko[2,4], Chris Q. Doe[1]*

[1]Institute of Neuroscience, Howard Hughes Medical Institute, University of Oregon, Eugene, OR 97403, USA
[2]Department of Genetics, Howard Hughes Medical Institute, Harvard Medical School, Boston, MA 02115, USA
[3]Institute of Developmental Biology and Neurobiology, Johannes-Gutenberg University Mainz, Mainz, Germany
[4]Department of Ophthalmology, Harvard Medical School, Boston, MA 02115, USA

* Co-authors for correspondence at cxu3@uoregon.edu or cdoe@uoregon.edu

Key words: visual system, lamina, homeodomain transcription factors, bipolar cells, LPCs, Scro

Short title: Homeodomain Cascade Drives Subtype Diversification

ABSTRACT

How a limited progenitor pool generates neuronal diversity remains a longstanding question. In the *Drosophila* lamina, a single progenitor type generates five lamina neuron subtypes—second-order neurons downstream of photoreceptors. Here, we identify a pan-class homeodomain transcription factor (HDTF), induced by Hedgehog signaling in progenitors and maintained across all five subtypes, that drives diversification within the progenitor-defined lamina class. This pan-class HDTF orchestrates a four-step program across the progenitor-to-newborn neuron transition: establishing progenitor identity, promoting cell-cycle exit, inducing subtype-specific differentially expressed (DE) HDTFs, and acting as their obligate cofactor to specify distinct subtypes. Loss of DE-HDTFs in newborn—but not older—neurons causes subtype-specific fate conversions at molecular, morphological, and functional levels, thereby reducing diversity. Notably, we find that mouse retinal neurons express analogous pan-class and DE-HDTFs, indicating evolutionary conservation. Our findings define a generalizable progenitor-to-newborn neuron HDTF cascade by which progenitor identity directs subtype diversification within a neuronal class.

INTRODUCTION

The brain comprises an extraordinary array of neuron types, each type characterized by identity features such as dendritic architecture, axonal projections, synaptic specificity, and neurotransmitter profiles[1–4]. These properties enable the precise neural processing underlying cognition and behavior.

Loss of specific neuronal populations often leads to irreversible neurological disorders, as exemplified by retinal ganglion cell degeneration in glaucoma[5] or dopaminergic neuron loss in Parkinson's disease[6]. Elucidating how neuronal diversity emerges during development is therefore a critical goal in neuroscience with profound implications for precision cell-replacement therapies.

Spatial and temporal factors specify progenitor identity and competence, thereby shaping neuronal output and contributing to neuronal diversity. In *Drosophila*, work in the optic lobe and embryonic ventral nerve cord has shown that spatial and temporal transcription factors (TFs) act combinatorially to specify progenitor identity, which in turn determines the types of neurons produced[7–9]. A classic example is neuroblast NB7-1, where the early temporal TF Hunchback specifies the first-born neurons: motor neurons U1 and U2 and their Notch-ON sibling interneurons[9]. In the mouse ventral neural cord, graded Sonic Hedgehog (Shh) signaling contributes to distinct combinatorial patterns of homeodomain TFs (HDTFs) in progenitors, thereby determining their neuronal output[10,11].

Nevertheless, a single progenitor identity can still yield diverse neuronal subtypes. In the mouse retina, Atoh7 expression in retinal progenitor cells confers competence to produce retinal ganglion cells (RGCs)—45 subtypes[12,13]—third-order projection neurons that transform bipolar input into feature-specific signals transmitted via the optic nerve to the brain[14]. Similarly, in the *Drosophila* lamina, a single progenitor type generates all five lamina neuron subtypes[15]—second-order neurons that process photoreceptor input and transmit signals to downstream neurons in the medulla. Thus, the capacity of individual progenitor types to generate diverse yet functionally related neuron subtypes is an essential feature of brain development. A critical question remains: how can a single progenitor class generate multiple neuronal subtypes?

We hypothesized that progenitor-derived pan-class HDTFs induce subtype-specific, differentially expressed (DE) HDTFs in newborn neurons and then act as their obligate cofactors to specify distinct subtypes within the progenitor-defined class. To test this hypothesis, we leveraged the genetic tractability of the *Drosophila* lamina, the first optic ganglion, where one progenitor type yields five lamina neuron subtypes[15]. We identify a pan-class HDTF that is initiated by Hedgehog (Hh) signaling in progenitors and maintained across all five subtypes. This pan-class HDTF drives diversification within the progenitor-defined lamina class by orchestrating a four-step program across the progenitor-to-newborn neuron transition. Moreover, we pinpoint the previously underappreciated newborn-neuron stage as a pivotal window in which progenitor-derived programs are interpreted, thereby determining future gene-expression profiles and functional properties of mature neurons. Notably, analogous pan-class and DE-HDTFs in mouse retinal neurons suggest an evolutionarily conserved framework by which progenitor identity directs subtype diversification within a single neuronal class.

RESULTS

A progenitor-derived, Hh-induced HDTF is uniformly expressed, while DE-HDTFs are subtype-specific in newborn neurons

During late larval and early pupal stages, photoreceptor axons deliver Hh to lamina precursor cells (LPCs), inducing expression of the TF Dachshund (Dac) and triggering their terminal division[16,17] (Figure 1A). Following division, postmitotic LPCs align with photoreceptor axons to form columns and differentiate into the five lamina neuron subtypes (L1-L5) within each of the ~800 cartridges[16]. LPCs are broadly marked by the nuclear receptor Tailless (Tll)[18], facilitating identification of this population. The lamina contains, within one tissue, a spatial continuum from LPCs to newborn and older neurons (Figure 1A), providing a powerful model for dissecting molecular events across the progenitor-to-neuron transition.

To identify candidate HDTFs acting in newborn lamina neurons, we first profiled HDTF expression across adult lamina neurons by single-cell RNA sequencing (scRNA-seq) (Figure 1B and 1C). This analysis identified candidate pan-class HDTFs, expressed across all five lamina neuron subtypes (pan-LN), as well as DE-HDTFs restricted to specific subtypes (Figure 1C).

We next asked whether candidate pan-LN HDTFs are expressed during lamina neurogenesis. Scarecrow (Scro) showed a spatiotemporal pattern resembling Dac: Scro was initiated in mitotic LPCs marked by phospho-Histone H3 (PH3) and persisted in postmitotic LPCs and all lamina neurons (Figure 1D). This suggested that Scro expression may be initiated by Hh signaling. Indeed, blocking Hh activity, using a temperature-sensitive loss-of-function allele (hh^{ts}), abolished Scro initiation in homozygous mutants (hh^{ts}/hh^{ts}), whereas heterozygous controls ($hh^{ts}/+$) exhibited normal Scro expression (see Methods) (Figure 1E). The absence of Scro was accompanied by disrupted lamina columns, labeled by horseradish peroxidase (HRP), due to loss of lamina neurogenesis[17] (Figure 1E). Scro expression persisted from the newborn-neuron stage into adulthood (Figure S1A and S1C). Thus, Scro is an Hh-induced, progenitor-derived pan-LN HDTF that is initiated in mitotic LPCs and maintained in all lamina neurons. The candidate pan-LN HDTFs Onecut and Zfh2 were not detected during neurogenesis and were excluded from further analysis (Figure S2A and S2B).

We next examined candidate DE-HDTFs during lamina neurogenesis. Consistent with our previous findings[18], Zfh1 was expressed in newborn L1 and L3 neurons, and Bsh in newborn L4 and L5 neurons (Figure 1F). By contrast, Ap and Pdm3 were initiated in older L4 and L5 neurons[18]. To identify an L2-specific DE-HDTF, we analyzed a published developing-lamina scRNA-seq dataset[19] and identified Defective proventriculus (Dve), a previously unreported lamina HDTF. Immunostaining detected Dve protein in newborn L2 and through 2 days after pupal formation (APF), but not at 3 days APF or in adults (Figure 1F, S1B, and S1C). Dve protein was also transiently detected in L5 around 2 days APF but was absent from newborn L5 (Figure S1B and S1C). DE-HDTF expression pattern mapped onto a stereotyped spatial arrangement of newborn lamina neuron somata: the distal layer contained Dve-positive L2 neurons, and intermediate layers contained Zfh1-positive L1/L3 neurons, and proximal layers contained Bsh-positive L4/L5 neurons (Figure 1F). At later stages, L2 and L3 somata became intermingled (Figure 1F). These findings define Zfh1, Dve, and Bsh as subtype-specific DE-HDTFs for newborn L1/L3, L2, and L4/L5, respectively (Figure 1G).

In summary, Scro is an Hh-induced, progenitor-derived pan-LN HDTF initiated in mitotic LPCs and maintained in all lamina neurons. DE-HDTFs are subsequently activated in newborn neurons in subtype-specific patterns, marking lamina neuron subtypes (Figure 1G). These findings suggest that Scro may function upstream of DE-HDTFs, promoting LPC cell-cycle exit and initiating DE-HDTF expression in newborn neurons to drive lamina neuron diversification (Figure 1H).

Pan-LN HDTF Scro promotes progenitor cell-cycle exit and initiates DE-HDTF expression in newborn neurons

During lamina neurogenesis, LPCs arise from Homothorax-positive (Hth^+) neuroepithelial progenitors, in which Hth sustains growth and proliferation[20]. Hh signaling represses Hth, which is initially retained in LPCs, and triggers their terminal division; this repression requires Hh-induced Dac[17,20].

Here, we identified Scro, a pan-LN HDTF, as another Hh-induced factor in LPCs. To test its function, we knocked down Scro (Scro-KD) specifically in LPCs and their lamina-neuron progeny (see Methods). Scro-KD nearly abolished Scro expression in both LPCs and lamina neurons (Figure 2A). Knockdown caused a striking expansion of Tll^+ LPCs before their assembly into HRP-labeled columnar structures, accompanied by a substantial reduction in lamina neurons, indicative of impaired neurogenesis (Figure 2A). Consequently, HRP^+ lamina columns were significantly smaller, consistent with reduced neuron production and LPC accumulation (Figure 2A). Expanded LPCs retained the mitotic marker phospho-Histone H3 (PH3), indicating that Scro is required for LPC cell-cycle exit (Figure 2A).

In Scro-KD, Dac was induced in LPCs and maintained in lamina neurons, and Hth was initially retained in LPCs and subsequently repressed, as in controls (Figure 2A and S3). Thus, Hth and Dac expression were unchanged in Scro-KD, indicating that Scro is not required for Dac expression or for repression of Hth. Given that Hh induces both Dac and Scro in LPCs, these results are consistent with two models: (i) parallel branches downstream of Hh, in which Dac mediates Hth repression while Scro promotes cell-cycle exit; or (ii) a linear pathway in which Dac acts upstream of Scro to promote cell-cycle exit (Figure 2A). Consistent with this framework, previously described hypomorphic *scro* mutants lack lamina neurons[21], and our data provide a mechanistic basis implicating failed LPC cell-cycle exit (Figure 2A).

Despite these defects, ~50% of the normal number of lamina neurons were still generated in Scro-KD animals (Figure 2A), likely due to the delayed onset of knockdown that allowed some LPCs to exit mitosis before substantial Scro depletion. We leveraged this residual neurogenesis to test whether Scro initiates DE-HDTF expression in newborn neurons. In controls, DE-HDTFs displayed subtype-specific expression: Zfh1 in L1 and L3, Dve in L2, and Bsh in L4 and L5 (Figure 2B). Scro-KD nearly abolished expression of all three in newborn lamina neurons, demonstrating that Scro is essential to initiate subtype-specific DE-HDTF expression (Figure 2B).

In the mature lamina, Scro-KD neurons lacking pan-LN and DE-HDTFs exhibited severe morphological defects. Their somata failed to segregate into discrete lamina layers, instead forming

aberrant clusters that often merged with medulla neuron somata (Figure 2C). Axonal targeting was profoundly altered: rather than projecting to superficial medulla layers (M1-M5), Scro-KD neurons extended axons broadly across all medulla layers (M1-M10) and into the lobula and lobula plate (Figure 2C).

Together, these results define a sequential requirement for the pan-LN HDTF Scro: first, to promote neurogenesis by triggering LPC cell-cycle exit, and subsequently, to initiate DE-HDTF expression in newborn neurons, thereby establishing neuronal identity features essential for proper lamina circuit integration. These data pinpoint the newborn-neuron stage as a critical window in which a progenitor-derived pan-LN HDTF launches the subtype-specific DE-HDTF program.

DE-HDTFs in newborn neurons diversify lamina neuron subtypes

We next asked whether DE-HDTFs act in newborn neurons to drive lamina neuron subtype diversification. As an initial test, we simultaneously knocked down two DE-HDTFs, Bsh and Dve (Bsh/Dve-DKD), reasoning that combined loss might unmask a default neuronal fate. In controls, the three DE-HDTFs showed mutually exclusive expression in newborn lamina neurons: Dve in distal-layer L2 neurons, Bsh in proximal-layer L4 and L5 neurons, and Zfh1 in intermediate-layer L1 and L3 neurons (Figure 3A). In Bsh/Dve-DKD animals, expression of Dve and Bsh was undetectable, and Zfh1 expanded across all newborn lamina neurons, indicating loss of L2, L4, and L5 identities (Figure 3A). As Zfh1 is required for generating L1 and L3 neurons[18], we asked whether ectopic Zfh1 is sufficient to drive L1 and L3 fates. Consistent with Zfh1 expansion, the L1 marker Svp and the L3 marker Erm became broadly expressed across all lamina layers, suggesting subtype conversion from L2, L4, and L5 to either L1 or L3 (Figure 3A). By 4 days APF, the mature lamina in Bsh/Dve-DKD animals comprised only L1 (~40%) and L3 (~60%) neurons, confirming persistent fate conversion (Figure S4A). Previously, we showed that Bsh loss alone converts L4 neurons to L3 and L5 neurons to L1[18]. Together, these findings indicate that the DE-HDTFs Bsh and Dve diversify lamina neuron subtypes by repressing default Zfh1-driven L1/L3 fates and promoting alternative fates. These observations are also consistent with an evolutionary scenario in which the ancestral lamina comprised only L1 and L3 neurons—responsive to increments and decrements of light intensity, respectively[22,23]—with subsequent diversification driven by the acquisition of Bsh and Dve (Figure 3C).

To determine the fate adopted by L2 neurons lacking only Dve, we performed lamina-specific Dve knockdown (Dve-KD). Dve-KD abolished Dve expression in L2 neurons and caused Zfh1 to expand into the distal L2 layer, suggesting an L2-to-L1 or L2-to-L3 fate switch (Figure 3B). Subtype marker analysis revealed ectopic Erm (L3 marker), but not Svp (L1 marker), confirming a specific L2-to-L3 conversion (Figure 3B). By 4 days APF, the mature lamina of Dve-KD exhibited an increased proportion of $Zfh1^{+}/Erm^{+}$ L3 neurons, accompanied by loss of the L2 marker Bab2, confirming stable L2-to-L3 conversion (Figure S4B).

Finally, we asked whether DE-HDTFs act specifically at the newborn-neuron stage to specify neuron subtype. The distinct temporal expression of Dve provided a unique opportunity to address

this question. Dve is transiently expressed in both L2 and L5 neurons, but at different developmental stages: in newborn L2 neurons, and in immature L5 around 2 days APF, but notably not in newborn L5 (Figure 1E and S1B). Bsh is expressed in newborn L5, and we previously showed that Bsh-KD converts L5 neurons to L1. Here, L5-specific Dve-KD abolished Dve expression but had no effect on the L5 marker Pdm3, indicating that Dve is dispensable for L5 specification (Figure S5A). Conversely, Pdm3-KD eliminated Dve expression in L5 neurons, placing Pdm3 upstream of Dve and confirming that late-stage Dve expression occurs downstream of subtype specification (Figure S5A and S5B).

Collectively, our findings demonstrate that DE-HDTFs in newborn neurons diversify lamina neuron subtypes by repressing default Zfh1-driven identities and promoting alternative fates (Figure 3C). These data establish the newborn-neuron stage as a pivotal window for neuron subtype specification.

Loss of DE-HDTFs converts lamina neuron subtypes morphologically and functionally

Loss of Dve converts L2 neurons into L3 based on molecular markers, prompting us to test whether this conversion also encompasses both morphological and functional characteristics. To examine morphology, we genetically labeled L3 neurons with membrane-targeted tdTomato. In adult controls, a single L3 neuron localized to each cartridge edge, extended neurites toward the cartridge core, and projected axons to medulla layer M3 (Figure 4A). In contrast, a single L2 neuron occupied the cartridge center and projects to medulla layer M2[24,25]. In Dve-KD animals, L3 neuron number nearly doubled, with each cartridge containing one endogenous and one ectopic L3 neuron (Figure 4A). Both endogenous and ectopic L3 neurons in Dve-KD occupied cartridge edges, extended neurites into the core, and projected axons to M3, indicating acquisition of canonical L3 morphology and loss of L2 morphology (Figure 4A). Overall axonal targeting remained intact, but terminals in Dve-KD animals appeared broader with occasional fine neurites extending into deeper medulla layers (Figure 4A), likely due to spatial constraints imposed by the doubled L3 population.

We next asked whether these ectopic L3 neurons also acquire L3 functional properties. Although both L2 and L3 neurons respond to light decrements, L2 responses are transient and contrast-sensitive, whereas L3 responses are sustained and luminance-sensitive[26–28]. To assess temporal profiles, we expressed the genetically encoded calcium indicator GCaMP6f in L3 neurons and recorded calcium signals from their axon terminals *in vivo* using two-photon imaging during visual stimulation. In response to a 5-second full-field flash (100% contrast), control L3 neurons showed sustained responses, whereas L2 neurons showed transient responses (Figure 4B; Movie S1 and S3). Upon Dve-KD, all labelled L3 neurons exhibited sustained responses similar to L3 controls (Figure 4B; Movie S1 and S2). Because each medulla column in Dve-KD animals contains both an endogenous and an ectopic L3 neuron, we placed regions of interest (ROIs) on individual axon terminal branches within individual columns to capture single-neuron responses from each. All ROIs responded robustly to the stimulus, with sustained profiles indistinguishable from control L3 neurons, showing that ectopic L3 neurons adopt the L3 sustained response property (Figure S6A).

We then tested luminance sensitivity, a defining property of L3 physiology[26,28]. We used a luminance-contrast discrimination stimulus[28] (Figure 4C) in which A steps varied in both luminance and contrast, and B steps were fixed at 25% contrast but varied in luminance. L2 neurons responded transiently and equally to all B steps, consistent with contrast sensitivity (Figure 4C). In contrast, all L3 neurons—both endogenous and ectopic—in Dve-KD animals exhibited sustained responses whose amplitudes scaled with luminance, matching the luminance sensitivity of control L3 neurons but distinct from the contrast sensitivity of L2 neurons (Figure 4C). Finally, using a randomized 11-level luminance stimulus, we found that all L3 neurons in Dve-KD exhibited nonlinear encoding of luminance information, consistent with the response property of control L3 neurons (Figure S6B).

Taken together, these data demonstrate that loss of Dve converts L2 neurons into morphologically and functionally bona fide L3 neurons, fully integrated into visual circuitry and displaying canonical L3 temporal and luminance-sensitive response properties.

Pan-LN and DE-HDTFs act combinatorially to specify lamina neuron subtypes

Co-expression of pan-LN and DE-HDTFs in newborn neurons suggested that progenitor-derived pan-LN HDTF could act as a required cofactor for DE-HDTFs to specify distinct subtypes, thereby driving diversification within the progenitor-defined lamina class. We used L5, a genetically tractable lamina subtype, as a representative to test this hypothesis. L5 specification requires the DE-HDTF Bsh, and loss of Bsh converts L5 neurons to L1, establishing its necessity for L5 fate[18]. To test whether the pan-LN HDTF Scro functions cooperatively with Bsh, we selectively knocked down Scro in L5 neurons after the onset of Bsh expression, thus keeping Bsh expression intact while depleting Scro during the newborn-neuron stage.

In controls, GFP-labeled L5 neurons co-expressed Scro and Bsh from the newborn-neuron stage, segregated into a discrete soma layer, and subsequently activated the L5-specific HDTF Pdm3 (Figure 5A). In contrast, newborn Scro-knockdown (Scro-KD) neurons transiently expressed Scro prior to RNAi-mediated depletion, retained Bsh, but failed to activate Pdm3 (Figure 5A). These neurons formed disorganized soma clusters intermingled with neighboring L4 cell bodies rather than segregating into the characteristic L5 layer, indicating that Scro is essential for initiating L5-specific marker expression and proper cell body positioning (Figure 5A and 5B).

In adults, Scro-KD neurons did not acquire characteristic L5 morphological features. In controls, L5 neurons lacked neurites spanning the lamina and projected axons into two superficial medulla layers (M1 and M5), whereas Scro-KD neurons extended ectopic neurites throughout the lamina and projected aberrant axonal extensions into deeper medulla layers (Figure 5C and S7). Notably, knocking down Pdm3 alone generated the axonal misprojection phenotype but did not disrupt soma organization or induce ectopic neurite extension within the lamina (Figure 5C and S7). This observation suggests that Scro regulates additional downstream targets beyond Pdm3 that are required for complete L5 morphogenesis (Figure 5D).

Together, these findings demonstrate that Scro and Bsh cooperatively specify L5 neuron identity at the newborn-neuron stage. They support a model in which progenitor-derived pan-LN

HDTF induces subtype-specific DE-HDTFs and acts as their obligate cofactor in newborn neurons to specify distinct subtypes, thereby driving diversification within a progenitor-defined lamina class (Figure 2B and 5B).

Conservation of pan-class and DE-HDTF expression in the mouse retina

To determine whether the Hh-induced HDTF cascade that directs subtype diversification within a neuronal class in the *Drosophila* lamina is conserved in mammals, we examined the mouse retina. Between embryonic day 11 and postnatal day 7, retinal progenitor cells generate six major retinal neuron classes—retinal ganglion cells (RGCs), cones, amacrine cells (ACs), horizontal cells (HCs), rods, and bipolar cells (BCs) (Figure 6A). During this neurogenic period, retina progenitor cells receive Sonic Hedgehog (Shh) signaling[29,30], suggesting that, analogous to *Drosophila*, Shh may initiate HDTF cascades essential for neuronal diversification.

We first asked whether BCs co-express pan-class and DE-HDTFs. Analysis of published scRNA-seq data[31] from mature BCs revealed that all 15 BC subtypes uniformly express the pan-BC HDTFs Otx2 and Vsx2[12] (Figure 6B). By contrast, BC subtypes differentially expressed distinct sets of DE-HDTFs, including established subtype markers Lhx3, Lhx4, Meis2, Irx5, Vsx1, Isl1, and Zeb2[12,32–36] (Figure 6B). Using *in situ* hybridization chain reaction (HCR) on postnatal day 18 retinas, we validated the differential expression of these DE-HDTFs within subsets of Vsx2+ or Otx2+ BCs (Figure 6C; Table S1). We also identified previously unreported HDTFs—Sebox, Six3, and Zfhx4—in subsets of Vsx+ or Otx2+ BC neurons in the inner nuclear layer (INL) (Figure 6C). Although Vsx2 is also expressed in Müller glia, these populations occupy distinct INL regions, with BC cell bodies located near the outer plexiform layer (OPL) and Müller glia situated centrally[32]. Notably, Sebox and Six3 transcripts localized to Vsx2+ cells adjacent to the OPL, confirming their BC-specific expression (Figure 6C).

To investigate whether the HDTF expression logic extends to other retinal neuron types, we analyzed a recently published single-cell atlas of the adult mouse retina[37]. All major retinal neuron types —cones, rods, HCs, RGCs, and ACs—expressed distinct combinations of HDTFs (Figure 6D–6G). RGCs and ACs, which exhibit extensive subtype diversity (45 and 63 subtypes, respectively)[37], co-expressed candidate pan-class HDTFs alongside subtype-specific DE-HDTFs (Figure 6D and 6G).

Together, these findings demonstrate that mouse retinal neurons, like *Drosophila* lamina neurons, co-express pan-class and DE-HDTFs. This cross-species convergence supports a conserved regulatory logic by which progenitor identity directs subtype diversification within a neuronal class (Figure 7).

DISCUSSION

Hedgehog Signals and Neural Progenitor Identity

Neural progenitors respond to extrinsic or intrinsic cues to produce diverse neuron types. For example, in the *Drosophila* embryonic ventral nerve cord, secreted Wingless and Hh proteins specify neuroblast identities[38–41]. Similarly, in the mouse ventral neural tube, graded Shh signaling defines distinct neural progenitor domains by directing combinatorial HDTF expression[10,42]. Shh signaling also drives the production of dopaminergic[43] and serotonergic neurons[44] in the mouse midbrain and hindbrain, respectively, likely by defining progenitor identities.

Previous work showed that Hh secreted from photoreceptors is required for LPCs to undergo terminal division[16]. Here, we extend these findings by demonstrating that Hh signaling activates the pan-LN HDTF Scro in LPCs, promoting cell-cycle exit and initiating expression of DE-HDTFs—Zfh1, Dve, and Bsh—in newborn neurons to drive lamina neuron subtype diversification. Whether this Hh-dependent HDTF cascade is conserved in other neural systems remains an important question. Notably, in the mouse retina, progenitors receive Shh signals from early-born retinal ganglion cells (RGCs)[45], and retinal neurons exhibit a similar pan-class and DE-HDTF expression pattern, supporting evolutionary conservation. Given that retinal progenitors and other neural progenitors sequentially express temporal TFs, future studies should investigate how Hh signals integrate with temporal TF programs to generate neuronal diversity.

Newborn Neurons: A Key Stage for Generating Neuronal Diversity

Temporal transcriptomic profiling across neuronal development—from progenitors to mature neurons—in systems such as the *Drosophila* visual system, mouse retina, neocortex, and somatosensory neurons has revealed the progressive emergence of transcriptionally distinct neuron types and identified candidate regulators of this diversification[46–49]. However, most analyses have focused on developing[46–52] or mature neurons[53,54], rather than newborn neurons, emphasizing how their differentially expressed genes contribute to morphological and functional specialization. Newborn neurons have received limited attention, partly because their transcriptomes and morphology appear uniform—they have not yet developed dendrites, axons, or synapses.

Despite their apparent uniformity, subtle molecular differences among newborn neurons can critically influence their subsequent differentiation. For instance, transient Notch signaling in newborn neurons governs binary fate decisions[55–57]. In the *Drosophila* lamina, we find that, in newborn neurons, progenitor-derived pan-class HDTF both induces subtype-specific DE-HDTFs and acts as their required partner to specify distinct lamina neuron subtypes. Loss of DE-HDTFs during the newborn-neuron stage— but not at later—causes subtype-specific fate conversions at molecular, morphological, and functional levels, underscoring a temporally restricted requirement for DE-HDTFs in subtype specification. Our previous work[58] further shows that Notch signaling integrates with HDTF activity to diversify neuronal fates (Figure 7). Defining the molecular logic that integrates Notch signaling with HDTF activity in newborn neurons will be critical. Together, these findings highlight the newborn-neuron stage as a pivotal window in which progenitor-derived programs are interpreted, thereby determining future gene-expression profiles and functional properties of mature neurons.

Diversifying subtypes within a neuronal class via pan-class and DE-HDTFs

While spatial factors and temporal TFs endow progenitors with the capacity to produce diverse neuron types[7,9], a key gap remains: how can a single progenitor identity generate multiple subtypes within one neuronal class, yielding distinct yet functionally related neurons? Here, in *Drosophila*, we identify an HDTF cascade acting across the progenitor-to-newborn neuron transition that drives neuronal diversification within a progenitor-defined class. We also uncover an analogous pan-class/DE-HDTF expression logic in the mouse retina. For instance, RGCs, which comprise ~45 distinct subtypes, co-express candidate pan-RGC HDTFs together with subtype-specific DE-HDTFs, consistent with a conserved within-class diversification strategy.

Several fundamental questions arise. Do pan-class HDTFs originate in retinal progenitor cells, and which upstream signals initiate their expression? Do pan-class HDTFs activate DE-HDTFs in newborn neurons, as seen for Scro in the lamina? Are both pan-class and DE-HDTFs required to specify individual RGC subtypes? And finally, do DE-HDTFs diversify RGCs from a common transcriptional ground state?

Our *Drosophila* data suggest a model in which the pan-LN HDTF Scro initiates neuronal diversification by selectively activating Zfh1, Dve, and Bsh in distinct newborn neuron populations. The basis of this selectivity is an important open question. The ectopic expression of Zfh1 upon Dve or Bsh knockdown suggests that these DE-HDTFs repress Zfh1. This repression could occur either through direct transcriptional repression by Dve and Bsh or via long-range chromatin interactions, akin to regulatory mechanisms governing Hox gene clusters and olfactory receptor loci[59–61].

Given the broad expression of HDTFs throughout the nervous system[62–64], our findings define a generalizable progenitor-to-newborn neuron HDTF cascade by which progenitor identity directs subtype diversification within a neuronal class.

Limitations of the study

We find that Scro is required to activate three DE-HDTFs—Dve, Bsh, and Zfh1—and that knockdown of Dve or Bsh induces ectopic Zfh1, consistent with repression of Zfh1 by both factors. Whether these regulatory relationships are direct remains unresolved; we did not map Scro, Dve, or Bsh binding at the relevant cis-regulatory elements. Future work, including CUT&RUN and 3D-genome-interaction assays (e.g., Hi-C), will be needed to address these questions. Additionally, scRNA-seq-derived HDTF expression list can include false negatives and false positives, for example, failure to recover Dve in L2 and spurious assignment of Zfh2 to lamina neurons. Therefore, our mouse retinal HDTF expression dataset will require further validation.

RESOURCE AVAILABILITY

Lead contact

Further information and requests for resources and reagents should be directed to, and will be fulfilled by, the lead contact, Chris Doe (cdoe@uoregon.edu).

Materials availability

Further information and requests for resources and reagents should be directed to the lead contact.

Data and code availability

The RNA-seq data reported in this paper have been deposited at GEO under accession number GSE305551 and are publicly available as of the date of publication. All original code has been deposited at [www.github.com/pnewstein/multi-species-homeodomain] and is publicly available.

ACKNOWLEDGMENTS

We thank Lawrence Zipursky for sharing published and unpublished reagents. We thank Claude Desplan, Makoto Soto, Richard Mann, James Skeath, Jing Peng, and Cheng-Ting Chien for reagents. Antibodies obtained from the Developmental Studies Hybridoma Bank, created by the NICHD of the NIH and maintained at the University of Iowa, Department of Biology, Iowa City, IA, were used in this study. Stocks obtained from the Bloomington Drosophila Stock Center (NIH P40OD018537) and Vienna Drosophila Resource Center were used in this study. We thank Ben Brissette, Kristen Lee, and Minoree Kohwi for comments on the manuscript.

This article is subject to HHMI's Open Access to Publications policy. HHMI lab heads have previously granted a nonexclusive CC BY 4.0 license to the public and a sublicensable license to HHMI in their research articles. Pursuant to those licenses, the author-accepted manuscript of this article can be made freely available under a CC BY4.0 license immediately upon publication.

AUTHOR CONTRIBUTIONS

CX conceived the project, performed and analyzed all experiments except neuron function assays, and wrote the manuscript with feedback from all authors. RGS performed and analyzed experiments. PN analyzed scRNA-seq data and designed HCR probes. RND helped perform mouse experiments. NW and MS performed and analyzed neuron function assays and contributed to the associated figures and text. CLC provided feedback on mouse experiments. CQD provided feedback during the project, contributed to writing the paper and assembling the figures. Funding was provided by HHMI (CQD, CLC) and from the European Research Council through the ERC grant 'Adaptive Vision', agreement No. 101045003 (MS). All authors commented on and approved the final manuscript.

DECLARATION OF INTEREST

The authors declare no competing financial or non-financial interests.

FIGURE LEGENDS

Figure 1. Hedgehog initiates Scro in mitotic LPCs, which is inherited by all newborn lamina neurons, while DE-HDTFs Zfh1, Dve, and Bsh are initiated in distinct subsets of newborn lamina neurons.

(A) Schematic diagram of lamina neurogenesis during later larval and early pupal stages. Photoreceptor axons deliver hedgehog (Hh) signals to lamina precursor cells (LPCs), triggering their terminal division. Dac is induced by Hh in LPCs and maintained in lamina neurons. Tailless (Tll) marks LPCs. The lamina, within one tissue, contains the full continuum from LPCs to newborn and older neurons.

(B) Schematic diagram of adult *Drosophila* optic lobe.

(C) Single-cell RNA sequencing of adult lamina neurons (LNs) followed by identification of HDTFs across five LN subtypes. LNs are from 3-day-old adult female flies. UMAP: each point represents a single cell; colors indicate LN subtypes defined by Leiden clustering. HDTF expression list: circle size reflects the percentage of cells in each cluster expressing the gene; color indicates average normalized expression in positive cells.

(D) Pan-LN HDTF Scro is initiated in mitotic lamina precursor cells (LPCs) and maintained in all LNs, showing a pattern similar to Dac. Dac marks a subset of LPCs and all LNs; HRP labels photoreceptor axons. Tll: LPC marker; PH3: mitotic marker. Yellow outlines: Dac^+ LPCs and LNs; yellow squares: $PH3^+$ $Scro^+$ mitotic LPC.

(E) hh^{ts}/ hh^{ts} mutants fail to initiate Scro expression in LPCs. Yellow outlines: LPCs and LNs.

(F) Zfh1, Dve, and Bsh are expressed in distinct newborn LN populations: Dve in L2; Zfh1 in L1 and L3; Bsh in L4 and L5. Yellow dashed outlines: LNs; yellow circles indicate Zfh1+ glia.

(G) Schematic summary.

(H) Proposed model.

Scale bar, 10 μm; n ≥ 5 brains; sample age, 19h APF.

See also Figures S1 and S2.

Figure 2. Scro sequentially promotes lamina neurogenesis and initiates expression of Zfh1, Dve, and Bsh in newborn neurons

(A) Scro knockdown (Scro-KD) impairs LPC cell-cycle exit and reduces LNs. Scro-KD in LPCs and their neuronal progeny is achieved using 27G05-Gal4, tub-$Gal80^{ts}$, and Scro-RNAi. Tll: LPC marker; Elav: neuron marker; HRP: lamina columns. Dashed yellow outlines: LPCs outside columns; white outlines: LNs; orange circles: $PH3^+$ mitotic LPCs. Areas of LPCs outside columns and LNs are quantified. Sample age: 19h APF.

(B) Scro-KD prevents initiation of Zfh1, Dve, and Bsh in newborn LNs. Yellow dashed outlines: LNs; yellow circles: Zfh1+ glia. Percentages of Dve^+, $Zfh1^+$, and Bsh^+ LNs are quantified. Sample age: 19h APF.

(C) Scro-KD neurons exhibit morphological defects in the mature lamina. Arrow indicates LN somata fused with medulla neuron somata. N ≥ 5 brains; sample age: 4d APF.

483 Data are mean ± SEM; n = 5 brains in control and n = 4 brains in Scro-KD in (A); n = 5 brains in
484 both groups in (B); ***p<0.001, unpaired t-test. Scale bar, 10 μm.
485 See also Figure S3.
486
487 **Figure 3. DE-HDTFs in newborn neurons diversify lamina neuron subtypes.**
488 (A) Bsh/Dve double knockdown (Bsh/Dve-DKD) converts L2, L4, and L5 neurons into L1 and L3.
489 DKD is achieved using 27G05-Gal4 to drive Scro-RNAi and Dve-dsRNA. Elav: neuron marker;
490 Svp: L1 marker; Erm: L3 marker. Yellow outlines: LNs. LN area and percentages of L1/L3
491 ($Zfh1^+Elav^+$), L2 (Dve^+), and L4/L5 (Bsh^+) within LN area are quantified.
492 (B) Dve knockdown (Dve-KD) converts L2 neurons into L3. Dve-KD is achieved using 27G05-Gal4
493 to drive dsDve-RNA. Yellow dashed outlines: L1–L3 neurons; orange outlines: L2 neurons. The L1,
494 L2, and L3 neuron area, percentages of L2 ($Elav^+$ $Zfh1^-$) and L1/L3 ($Zfh1^+$) within L1/L2/L3 area,
495 and percentages of L1 (Svp^+), L2 (Dve^+), and L3 (Erm^+) within L1/L2/L3 area are quantified.
496 (C) Schematic summary. Our previous work shows that Bsh knockdown induces ectopic Zfh1 and
497 converts L4 and L5 neurons into L3 and L1, respectively[18].
498 Data are mean ± SEM; n = 5 brains in (A) and (B); ns, not significant; ***p<0.001, unpaired t-test.
499 Scale bar, 10 μm; sample age: 19h APF.
500 See also Figures S4 and S5.
501
502 **Figure 4. Converted L3 neurons from L2 adopt L3-like morphology and function.**
503 (A) L2-to-L3 converted neurons in Dve-KD animals adopt L3-like dendritic arbors and axonal
504 targeting. Each cartridge contains one endogenous and one ectopic L3 in Dve-KD. Dve-KD is driven
505 by 27G05-Gal4 with Dve-dsRNA. L3 neurons are labeled using 22E09-LexA>LexAop-
506 myr::tdTomato. Chaoptin labels all photoreceptors and delineates medulla layers M3 and M6.
507 Dashed circles: individual lamina cartridges; pink circles: L3 neurite shafts. The percentage of L3
508 neurons within LNs is quantified. Data are mean ± SEM; n = 5 brains; ***p<0.001, unpaired t-test.
509 The number of L3 neurons per cartridge is also quantified (control: n = 133 cartridges from 6 brains;
510 Dve-KD: n = 142 cartridges from 6 brains); ***p<0.001, permutation test. Scale bar, 10 μm; sample
511 age: 1-d adult.
512 (B) L2-to-L3 converted neurons in Dve-KD animals exhibit L3-like sustained responses rather than
513 L2 transient responses. Dve-KD is driven by 27G05-Gal4 with Dve-dsRNA. In L3 neurons,
514 GCaMP6f expression is driven by 22E09-LexA; in L2 neurons, by 16H03-LexA. Representative
515 images of L3 neurons expressing the genetically encoded calcium indicator GCaMP6f in control and
516 Dve-KD animals. Scale bar, 10 μm. Average calcium traces recorded from L3 axonal terminals in
517 response to full-field flashes (FFF) for control (green), Dve-KD (grey), and L2 control (blue)
518 animals. Quantification of the percentage of peak response retained at the plateau of the OFF step for
519 the FFF response for control, n = 13 (297 ROIs); Dve-KD, n = 9 (381 ROIs); L2 control, n = 7 (465
520 ROIs); ns, not significant, ***p<0.001, unpaired t-test. Scale bar, 10 μm; sample age: 5-7 d adult.
521 (C) L2-to-L3 converted neurons in Dve-KD animals exhibit L3-like luminance sensitivity rather than
522 L2 contrast sensitivity. Schematic of the A-B steps stimulus paradigm, showing sequential A- and B-

523 steps following a 30 s adapting stimulus. Average calcium traces are shown for control (n = 7, 49
524 ROIs; green), Dve-KD (n = 8, 37 ROIs; grey), and L2 control (n = 6, 80 ROIs; blue). Peak calcium
525 responses to A- and B-steps are plotted as a function of contrast across all conditions. Linear
526 regression models were fitted to assess response trends. Slopes from the regression models for peak
527 responses to B-steps are quantified for all conditions. ns, not significant, $**p < 0.01$, unpaired t-test.
528 sample age: 5-7 d adult.
529 See also Figure S6 and Movies S1-S3.
530
531 **Figure 5. Pan-LN HDTF Scro and DE-HDTF Bsh act combinatorially in newborn neurons to**
532 **specify L5 neurons.**
533 (A) Scro knockdown (Scro-KD) in newborn L5 neurons (using Bsh-L-Gal4>Scro-RNAi) results in
534 transient Scro expression prior to RNAi-mediated depletion. Bsh remains intact, but Pdm3 activation
535 is blocked. Bsh-LexA>LexAop-myr::GFP labels L5 neurons independently of fate. Pdm3: L5-
536 specific HDTF. White outlines: GFP^+ neurons. Sample age: 19h APF.
537 (B) Schematic model: Scro and Bsh cooperate to specify L5 neurons. Our previous work shows that
538 Bsh is required in newborn neurons to specify L5 identity[18].
539 (C) Scro-KD neurons exhibit ectopic neurites in the lamina and axonal misprojection in the medulla.
540 Pdm3 knockdown (Pdm3-KD), using Bsh-L-Gal4>Pdm3-RNAi-#1, partially phenocopies the
541 medulla projection defect. Yellow arrows highlight ectopic neurites in the lamina (Scro-KD) and
542 misprojected axons in the medulla (Scro-KD and Pdm3-KD). Sample age: 1-d adult.
543 (D) Schematic summary: Scro and Bsh act combinatorially to specify L5 morphology, in part
544 through Pdm3. Our previous work shows that Bsh is required for L5-specific morphology[18].
545 Scale bar, 10 μm; n ≥ 5 brains.
546 See also Figure S7.
547
548 **Figure 6. Mouse retinal neurons express pan-class and DE-HDTFs.**
549 (A) Schematic of the mouse retina.
550 (B) Expression of HDTFs across fifteen bipolar cell (BC) subtypes from published scRNA-seq
551 data[31] (P17). Circle size: % of cells in each subtype expressing the gene; color: average normalized
552 expression in positive cells.
553 (C) Validation of pan-BC and DE-HDTF expression in P18 retinas using *in situ* hybridization chain
554 reaction (HCR). Yellow circles: $DE\text{-}HDTF^+$ BC somata.
555 (D-G) Expression of HDTFs in cones, rods, horizontal cells (HCs), retinal ganglion cells (RGCs),
556 and amacrine cells (ACs) from a published single-cell atlas of the adult mouse retina[37].
557 Scale bar, 10 μm; n = 3 mice.
558 See also Table S1.
559
560 **Figure 7. Model: pan-class and DE-HDTFs diversify subtypes within a neuronal class.**
561 *Drosophila* (left): Hh signaling induces the pan-class HDTF Scro in LPCs, promoting cell-cycle exit.

562 Scro is inherited by all newborn lamina neurons (LNs), where it activates DE-HDTFs—Dve, Zfh1,
563 and Bsh—and acts as their cofactor to specify distinct LN subtypes.
564 Mouse retina (right): Analogous pan-class and DE-HDTFs are expressed in retinal neurons. Using
565 bipolar cells (BCs) as an example, we propose that Shh induces the pan-BC HDTFs Otx2 and Vsx2
566 in retinal progenitor cells (RPCs), promoting cell-cycle exit. Otx2 and Vsx2 are maintained in
567 newborn BCs, where they activate DE-HDTFs and act as their cofactors to specify 15 BC subtypes.
568 N^{On}: Notch-on; N^{On}?: predicted Notch-on state.
569
570 **Figure S1. Transient expression of Dve in L2 and L5 neurons and persistent expression of Scro**
571 **in all lamina neurons, related to Figure 1.**
572 (A) Scro remains expressed in all LNs in adults. Elav labels LNs.
573 (B) Dve is expressed in L2 and L5 neurons at 2 days after pupal formation (2d APF) but becomes
574 absent by 3d APF and in adults.
575 (C) Schematic summary.
576 Scale bar, 10 μm; n ≥ 5 brains.
577
578 **Figure S2. Onecut and Zfh2 are not expressed in the lamina during neurogenesis, related to**
579 **Figure 1.**
580 (A) Onecut mRNA is not detected in the lamina using *in situ* hybridization chain reaction (HCR).
581 Svp and Erm are L1 and L3 markers, respectively.
582 (B) Zfh2 protein is not detected in lamina neurons during lamina neurogenesis. Tll marks LPCs.
583 Elav labels neurons. White outlines: $Zfh2^+$ cells.
584 Scale bar, 10 μm; n ≥ 5 brains; sample age: 19h APF.
585
586 **Figure S3. Hth expression is unchanged in Scro-KD, related to Figure 2.**
587 (A) As in controls, LPCs initially express Hth, which is subsequently silenced; this pattern is
588 unchanged in Scro-KD. Scro-KD in LPCs and their neuronal progeny is achieved using 27G05-
589 Gal4, tub-$Gal80^{ts}$, and Scro-RNAi. Tll: LPC marker; Elav: neuron marker; HRP: lamina columns.
590 Yellow dashed outlines: LPCs outside columns. Scale bar, 10 μm; sample age: 19h APF.
591
592 **Figure S4. DE-HDTFs diversify lamina neuron subtypes, related to Figure 3.**
593 (A) Bsh/Dve double knockdown (Bsh/Dve-DKD) results in a mature lamina containing only L1 and
594 L3 neuron subtypes. Elav labels neurons; Bab2: L2 marker; Svp: L1 marker; Erm: L3 marker.
595 Yellow outlines: LNs. Quantification: LN number; percentages of L1/L3 ($Zfh1^+$), L2 ($Bab2^+$), and
596 L4/L5 (Bsh^+) within the LN population; percentages of L1 (Svp^+) and L3 (Erm^+) within the LN
597 population.
598 (B) Dve knockdown (Dve-KD) results in a loss of L2 neurons and an increase of L3 neurons in the
599 mature lamina. Yellow dashed outlines: L1–L3 neurons. Quantification: L1/L2/L3 neuron number;
600 percentages of L1/L3 ($Zfh1^+$) and L2 ($Bab2^+$) within the L1/L2/L3 population; percentages of L1
601 (Svp^+) and L3 (Erm^+) within the L1/L2/L3 population.

Data are mean ± SEM; n = 6 brains in (A) and (B); ns, not significant; ***p<0.001, unpaired t-test. Scale bar, 10 µm; sample age: 4d APF.

Figure S5. Dve is not required for L5 specification, related to Figure 3.
(A) Dve knockdown (Dve-KD) in L5 neurons abolishes Dve expression in L5 neurons but does not affect Bsh or Pdm3 expression. Pdm3 expression becomes absent in Pdm3-knockdown (Pdm3-KD) animals. Pdm3-KD in L5 neurons is achieved using Bsh-L-Gal4 to drive Pdm3-RNAi-#2. White dashed outlines: L2 neurons; White outlines: L5 neurons.
(B) Schematic summary.
Scale bar, 10 µm; n≥5 brains; sample age: 53h APF.

Figure S6. Converted L3 neurons from L2 adopt L3-like sustained response and nonlinear luminance encoding, related to Figure 4.
(A) Regions of interest (ROIs) drawn on individual cartridges of L3 axon terminals in L3 control and Dve-KD animals. Average calcium response (orange) and individual ROI responses (black) to full-field flashes in L3 control (n = 18) and Dve-KD (n = 18) animals. Raw calcium traces from individual ROIs in response to full-field flashes in L3 control and Dve-KD animals. Scale-bar, 5 µm; sample age: 5-7 d adult.
(B) Representative calcium traces from a single ROI in response to the luminance-steps stimulus for L3 control (green), Dve-KD (grey), and L2 control (blue) animals. Plateau responses plotted as a function of luminance and fitted with exponential functions for L3 control (green), Dve-KD (grey), and L2 control (blue) animals. Quantification of decay rates for the fitted exponential functions: L3 control (n = 10, 82 ROIs; green), Dve-KD (n = 8, 78 ROIs; grey), and L2 control (n = 7, 115 ROIs; blue); *p<0.05, **p<0.01, Mann-Whitney U test. Mutual information between plateau response and luminance: L3 control (n = 10, 82 ROIs; green), Dve-KD (n = 8, 78 ROIs; grey), and L2 control (n = 7, 115 ROIs; blue); ns, not significant, **p<0.01, unpaired t-test. Sample age: 5-7 d adult.

Figure S7. Pdm3 expression is severely reduced in Scro-KD and Pdm3-KD L5 neurons, related to Figure 5.
(A) Scro knockdown (Scro-KD) in newborn L5 neurons is achieved using Bsh-L-Gal4 to drive Scro-RNAi. Pdm3 knockdown (Pdm3-KD) in L5 neurons is achieved using Bsh-L-Gal4 to drive Pdm3-RNAi-#1. Bsh-LexA and LexAop-my::GFP are used to trace L5 neurons independent of L5 fate. The Pdm3 signal intensity normalized to GFP is quantified.
Data are mean ± SEM; n = 5 brains, ***p<0.001, unpaired t-test. Scale bar, 10 µm; sample age: 1d adult.

STAR METHOD

KEY RESOURCES TABLE

REAGENT or RESOURCE	SOURCE	IDENTIFIER

Antibodies		
guinea pig polyclonal anti-Scro (1:600)	Gift from Lawrence Zipursky; unpublished antibody	N/A
guinea pig polyclonal anti-Hth (1:2000)	Gift from Richard Mann[65]	N/A
mouse monoclonal anti-Dac (1:100)	Developmental Studies Hybridoma Bank	Cat#mAbdac1-1, RRID: AB_579773
goat polyclonal anti-HRP TAG; Alexa Fluor® 405 (1:100)	Jackson ImmunoResearch Lab	Cat#123-475-021, RRID: AB_2632561
rabbit polyclonal anti-PH3 (1:1000)	Millipore Sigma	Product#04-817
rabbit polyclonal anti-Tailless (1:200)	Asian Distribution Center for Segmentation Antibodies	Code#812
mouse monoclonal anti-Elav (1:100)	Developmental Studies Hybridoma Bank	Cat#Elav-9F8A9, RRID: AB_528217
rat monoclonal anti-Elav (1:50)	Developmental Studies Hybridoma Bank	Cat#Rat-Elav-7E8A10 anti-elav, RRID: AB_528218
rabbit polyclonal anti-Bsh (1:1000)	Gift from Claude Desplan[48]	N/A
guinea pig polyclonal anti-Bsh (1:1000)	Gift from Lawrence Zipursky[19] & Makoto Soto[66]	N/A
rat monoclonal anti-Bsh (1:1000)	Chris Doe's Lab[58]	N/A
guinea pig polyclonal anti-Zfh1 (1:1000)	Gift from James Skeath[67]	N/A
rabbit polyclonal anti-Dve (1:1000)	Gift from Claude Desplan[68]	N/A
chicken polyclonal anti-GFP (1:1000)	Abcam	Cat#ab13970, RRID: 300798
rat monoclonal anti-Erm (1:70)	Gift from Jing Peng[69]	N/A
mouse monoclonal anti-Svp (1:6)	Developmental Studies Hybridoma Bank	Cat#Seven-up D2D3, RRID: 2618079
rabbit polyclonal anti-DS Red (1:150)	TaKaRa	Cat#632496
mouse monoclonal anti-chaoptin (1:10)	Developmental Studies Hybridoma Bank	Cat#24B10, RRID: AB_528161

rat monoclonal anti-Pdm3 (1:600)	Gift from Cheng-Ting Chien[70]	N/A
rat monoclonal anti-Zfh2 (1:250)	Chris Doe's Lab[71]	N/A
rabbit polyclonal anti-Bab2 (1:300)	This Paper	See methods section: Generating Bab2 antibody
Alexa Fluor 405 donkey anti-rat (1:400)	Jackson ImmunoResearch Lab	Cat#712-475-150, RRID: AB_2340680
Alexa Fluor 405 donkey anti-rabbit (1:400)	Jackson ImmunoResearch Lab	Cat#711-475-152, RRID: AB_2340616
Alexa Fluor 405 donkey anti-guinea pig (1:400)	Jackson ImmunoResearch Lab	Cat#706-475-148, RRID: AB_2340470
Alexa Fluor 488 donkey anti-rat (1:400)	Jackson ImmunoResearch Lab	Cat#712-545-153, RRID: AB_2340684
Alexa Fluor 488 donkey anti-chicken (1:400)	Jackson ImmunoResearch Lab	Cat#703-545-155, RRID: AB_2340375
Alexa Fluor 488 donkey anti-guinea pig (1:400)	Jackson ImmunoResearch Lab	Cat#706-545-148, RRID: AB_2340472
Alexa Fluor 488 donkey anti-rabbit (1:400)	Jackson ImmunoResearch Lab	Cat#711-545-152, RRID: AB_2313584
Alexa Fluor 488 donkey anti-mouse (1:400)	Jackson ImmunoResearch Lab	Cat#715-545-150, RRID: AB_2340846
Rhodamine Red-X donkey anti-mouse (1:400)	Jackson ImmunoResearch Lab	Cat#715-295-151, RRID: AB_2340832
Rhodamine Red-X donkey anti-rat (1:400)	Jackson ImmunoResearch Lab	Cat#712-295-153, RRID: AB_2340676
Rhodamine Red-X donkey anti-rabbit (1:400)	Jackson ImmunoResearch Lab	Cat#711-295-152, RRID: AB_2340613
Rhodamine Red-X donkey anti-guinea pig (1:400)	Jackson ImmunoResearch Lab	Cat#706-295-148, RRID: AB_2340468
Alexa Fluor 647 donkey anti-rabbit (1:400)	Jackson ImmunoResearch Lab	Cat#711-605-152, RRID: AB_2492288

Alexa Fluor 647 donkey anti-mouse (1:400)	Jackson ImmunoResearch Lab	Cat#715-605-151, RRID: AB_2340863
Alexa Fluor 647 donkey anti-guinea pig (1:400)	Jackson ImmunoResearch Lab	Cat#706-605-148, RRID: AB_2340476
Alexa Fluor 647 donkey anti-rat (1:400)	Jackson ImmunoResearch Lab	Cat#712-605-153, RRID: AB_2340694
Chemicals, peptides, and recombinant proteins		
Immunostain Enhancer	Fisher Scientific	Cat#PI46644
SSC X20	Fisher Scientific	Cat#AM9763
Triton X-100	Millipore Sigma	Cat#T8787-250ML
HCR RNA-FISH Kit (Probe Hybridization Buffer, Probe Wash Buffer, Amplification Buffer)	Molecular Instruments	N/A
405-Wheat Germ Agglutinin	Thermo Fisher	Cat#W56132
SlowFade™ Gold Antifade Mountant	Thermo Fisher	Cat#S36936
Deposited data		
scRNA-seq data of *Drosophila* lamina neurons	This paper	GEO: GSE305551
Experimental models: Fly stocks		
D. melanogaster: 10xUAS-IVS- myristoylated-GFP	Bloomington Drosophila Stock Center	RRID: BDSC_32198
D. melanogaster: 27g05Gal4	Bloomington Drosophila Stock Center	RRID: BDSC_48703
D. melanogaster: 27g05FLP	Bloomington Drosophila Stock Center	RRID: BDSC_55765
D. melanogaster: Bsh-L-Gal4	Gift from Makoto Sato[66]	N/A
D. melanogaster: Bsh-LexA	Bloomington Drosophila Stock Center	RRID: BDSC_52834
D. melanogaster: 22E09-LexA	Bloomington Drosophila Stock Center	RRID: BDSC_94644
D. melanogaster: Hedgehog (ts)	Bloomington Drosophila Stock Center	RRID: BDSC_1684
D. melanogaster: UAS-Scro-RNAi	Bloomington Drosophila Stock Center	RRID: BDSC_33890

D. melanogaster: UAS-Bsh-RNAi	Bloomington Drosophila Stock Center	RRID: BDSC_29336
D. melanogaster: UAS-Dve-dsRNA	Vienna Drosophila Resource Center	RRID: VDRC_109538
D. melanogaster: UAS-Pdm3-RNAi (#1)	Bloomington Drosophila Stock Center	RRID: BDSC_35726
D. melanogaster: UAS-Pdm3-RNAi (#2)	Bloomington Drosophila Stock Center	RRID: BDSC_53887
D. melanogaster: LexAop-IVS-myr::sfGFP	Bloomington Drosophila Stock Center	RRID: BDSC_32209
D. melanogaster: 13xLexAop2-IVS-GCaMP6f-p10	Bloomington Drosophila Stock Center	RRID: BDSC_44277
D. melanogaster: GMR16H03-LexA	Bloomington Drosophila Stock Center	RRID: BDSC_52510
D. melanogaster: LexAop-myrTdTom	Gift from Lawrence Zipursky[72]	N/A
D. melanogaster: tubP-Gal80[ts]	Bloomington Drosophila Stock Center	RRID: BDSC_7017
D. melanogaster: VALIUM20-mCherry	Bloomington Drosophila Stock Center	RRID: BDSC_35785
D. melanogaster: Oregon-R-C	Bloomington Drosophila Stock Center	RRID: BDSC_5
Oligonucleotides		
Drosophila HCR Probe Set for Onecut (B5)	Molecular Instruments	N/A
Drosophila HCR Probe Set for Erm (B2)	Molecular Instruments	N/A
Drosophila HCR Probe Set for Svp (B3)	Molecular Instruments	N/A
Custom Mouse HCR Probe Set	This paper; synthesized by Integrated DNA Technologies (IDT)	See Table S1
HCR Amplifier - B1-Alexa Fluor 488	Molecular Instruments	N/A
HCR Amplifier - B1-Alexa Fluor 546	Molecular Instruments	N/A

HCR Amplifier - B2-Alexa Fluor 546	Molecular Instruments	N/A
HCR Amplifier - B2-Alexa Fluor 647	Molecular Instruments	N/A
HCR Amplifier - B3-Alexa Fluor 488	Molecular Instruments	N/A
HCR Amplifier - B3-Alexa Fluor 546	Molecular Instruments	N/A
HCR Amplifier - B3-Alexa Fluor 647	Molecular Instruments	N/A
HCR Amplifier - B4-Alexa Fluor 647	Molecular Instruments	N/A
HCR Amplifier - B5-Alexa Fluor 488	Molecular Instruments	N/A
HCR Amplifier - B5-Alexa Fluor 647	Molecular Instruments	N/A
Software and algorithms		
Fiji	[73,74]	https://imagej.nih.gov/ij/download.html; RRID:SCR_002285
self-assembling-manifold	[75]	https://github.com/atarashansky/self-assembling-manifold; RRID:SCR_027330
scanpy	[76]	https://github.com/scverse/scanpy; RRID:SCR_018139
Prism	[77]	www.graphpad.com; RRID:SCR_002798
Ensembl	[78]	https://www.ensembl.org/biomart/martview/
Other		
Terasaki Plate	Greiner Bio-One	Cat#653180
96-Well Plate	Fisher Scientific	Cat#08-772-2C

EXPERIMENTAL MODEL AND SUBJECT DETAILS

All flies were reared at 25 °C on standard cornmeal fly food, unless otherwise stated. For all RNAi and dsRNA knockdown experiments, crosses were kept at 25 °C, and their progeny were kept at 28 °C with a 16:8 hours light-dark cycle from the second larval stage until dissection. For all Gal80^{ts} experiments, crosses were kept at 18°C, and progeny were kept at 29 °C at the desired time.

METHOD DETAILS

Animal collections

Hedgehog (Hh) loss-of-function

For the temperature-sensitive Hh loss-of-function experiment (*hh*^{ts}), animals were reared at 18 °C and shifted to 28 °C at the onset of wandering third-instar larvae (L3). Brains were dissected at 19 h after pupal formation (APF). *hh*^{ts}/TM6B served as controls; *hh*^{ts}/*hh*^{ts} were the loss-of-function genotype.

Conditional Scro knockdown in LPCs and progeny

For Scro-knockdown (Scro-KD) using 27G05-Gal4, tub-Gal80^{ts}, and UAS-Scro-RNAi, animals were reared at 18 °C and shifted to 29 °C at early L3 to permit Gal4-driven RNAi expression and initiate Scro depletion just before the lamina neurogenesis.

Bsh-KD, Dve-KD, and Bsh/Dve-DKD

For Bsh-KD, Dve-KD, and Bsh/Dve double knockdown (DKD) using 27G05-Gal4 with UAS-Bsh-RNAi and UAS-Dve-dsRNA, animals were reared at 25 °C and shifted to 28 °C at the second-instar larval stage.

Scro-KD in newborn L5 neurons

For Scro-KD with Bsh-L-Gal4 and UAS-Scro-RNAi, animals were reared at 25 °C and shifted to 29 °C at early L3.

scRNA-seq samples

Oregon-R flies were reared at 25 °C, and 3-day-old adult females were dissected for scRNA-seq.

Generating Bab2 antibody

Bab2 protein and antibody production were performed by GenScript (Piscataway, NJ) using rabbits immunized with the following portion of the Bab2 open reading frame:

RDPEHT ELRMCLEAKK SRSLPVSPQP QPNLKLAGSA LFEFGQRSSP VETKIKTNPE
TKPPRRKIVP PSGEGQQFCL RWNNYQSNLT NVFDELLQSE SFVDVTLSCE GHSIKAHKMV
LSACSPYFQA LFYDNPCQHP IIIMRDVSWS DLKALVEFMY KGEINVCQDQ INPLLKVAET
LKIRGLAEVS AGRGEGGASA LPMSAFDDED EEEELASATA ILQQDGDADP
DEEMKAKRPR LLPEGVLDLN QRQRKRSRDG SYATPSPSLQ GGESEISERG SSGTPGQSQS
QPLAMTTSTI VRNPFASPNP QTLEGRNSAM NAVANQRKSP APTATGHSNG
NSGAAMHSPP GGVAVQSALP PHMAAIVPPP PSAMHHHAQQ LAAQHQLAHS
HAMASALAAA AAGAGAAGAG GAGSGSGSGA SAPTGGTGVA GSGAGAAVG

691 ***Drosophila* Immunohistochemistry**

692

693 Fly brains were dissected in Schneider's medium and fixed in 4% paraformaldehyde (PFA) diluted
694 in phosphate-buffered saline (PBS) for 25 min. Following fixation, brains were briefly rinsed in PBS
695 containing 0.5% Triton X-100 (PBST) and then incubated in PBST for ≥4 hr at room temperature
696 (RT) in a 96-well plate. Samples were subsequently blocked overnight (O/N) at 4 °C in blocking
697 buffer (10% normal donkey serum, PBST). Brains were then incubated in primary antibody (diluted
698 in immunostain enhancer solution) at 4 °C for ≥2 nights. After four 25-min washes with PBST,
699 samples were incubated in secondary antibody (diluted in blocking buffer) at 4 °C for ≥1 day. After
700 secondary antibody incubation, brains were washed with PBST four times for 25 min each and
701 mounted in SlowFade Gold antifade reagent. Images were acquired using a Zeiss 800 confocal and
702 processed with Image J[73].

703

704 ***Drosophila* HCR-FISH**

705

706 The HCR-FISH protocol was adapted from Dombrovski et al.[79] with minor modifications. Following
707 dissection and fixation on ice, samples were rinsed three times with PBST and incubated in PBST
708 for 30 min on ice in a Terasaki plate. Samples were transferred to a 96-well plate and equilibrated in
709 pre-warmed probe hybridization buffer (PHB) for 30 min at 37 °C and then incubated O/N at 37 °C
710 in probes diluted in PHB (1 µL of 1 µM stock probe solution per 200 µL buffer).

711

712 The next day, the samples were washed four times with pre-warmed probe wash buffer (PWB) for
713 15 min at 37 °C, followed by two 5 min washes with SSCT buffer (20x SSC with 0.1% Triton X-
714 100) rotating at RT. Samples were equilibrated in HCR amplification buffer (AB) for 30 min,
715 rotating at RT. During this time, HCR Amplifiers were heat-activated in a thermal cycler (90 s at
716 95 °C), and then kept in the dark for 30 min at RT. The HCR Amplifiers were diluted in AB (2 µl of
717 each hairpin per 100 µl of buffer), and incubated the samples at RT O/N.

718

719 Following amplification, samples were washed four times with SCCT at RT: twice for 5 min and
720 twice for 30 min. Samples were mounted in SlowFade Gold antifade reagent and stored at 4 °C until
721 confocal imaging using a Zeiss 800 microscope. HCR-FISH was performed using HCR v3.0 probe
722 sets, which were designed and synthesized by Molecular Instruments; probe sequences are
723 proprietary and were not disclosed by the manufacturer.

724

725 ***Drosophila* scRNA-seq sample preparation**

726

727 Single-cell RNA sequencing (scRNA-seq) was performed using a protocol adapted from Peng et
728 al.[80] with minor modifications. Papain (100 U/ml in Complete Schneider's Medium, CSM) was
729 freshly prepared and activated at 37 °C for 30 min; Liberase TM aliquots were thawed at RT. Adult
730 brains were dissected in cold CSM, and optic lobes were pooled on ice in Rinaldini's Solution (RS).
731 For each dissociation, 300 µl activated papain was combined with 4.1 µl Liberase (0.18 WU/ml) to
732 prepare the dissociation solution. After a brief RS wash and removal, the dissociation solution was
733 added to the lobes and incubated at 25 °C with shaking (1000 rpm) for 15 min, with gently mixing at
734 5 min and 10 min. Lobes were washed twice with RS, followed by two washes with CSM, and then
735 gently triturated in fresh CSM to obtain a homogenous single-cell suspension. Suspensions were
736 passed through a 20 µm strainer into low-adhesion tubes on ice; the filter was rinsed with 500 µl

CSM. Cells were pelleted (300 × g, 5 min, RT), resuspended in PBSB (PBS + 0.04% BSA), and submitted immediately for 10x Genomics scRNA-seq. Solutions: CSM (50 mL): 5 mL heat-inactivated bovine serum; 0.1 mL insulin; 5 mL 200 mM L-glutamine; 12.5 µL 20 mg/mL L-glutathione; 39 mL Schneider's medium; 1 mL penicillin/streptomycin. RS (10× stock, 100 mL): 8 g NaCl; 200 mg KCl; 50 mg NaH_2PO_4; 1 g $NaHCO_3$; 1 g glucose. (Dilute to 1× before use.)

Drosophila scRNA-seq analysis

Gene-by-cell count matrices were generated with 10x Genomics Cell Ranger (v7.1.0). Quality control retained cells with 500–2,500 detected genes and ≤10% mitochondrial UMI fraction. Downstream preprocessing used the Self-Assembling Manifold (SAM) package[75] with default parameters for normalization, highly variable gene selection, and dimensionality reduction. Cells were clustered with the Leiden algorithm[81] (resolution = 1.0), and clusters corresponding to L1–L5 were annotated by canonical marker gene expression. Data were visualized using UMAP as implemented in Scanpy[76].

HDTF expression profiling (*Drosophila* and Mouse)

Drosophila lamina single-cell data were generated in this study; processing details are provided above. Mouse bipolar-cell scRNA-seq data were obtained from Shekhar et al. [82] and converted to AnnData using Scanpy[76]; scRNA-seq data for other retinal classes were obtained from Li et al.[37]. HDTFs were defined by SMART[83] or PANTHER[84] domain annotations accessed via Ensembl BioMart[85]. Dot-plot visualizations were produced with Scanpy[76]. Genes were retained if their mean normalized expression in any cell type within a class exceeded a prespecified threshold, and genes were ordered by the number of cell types within that class surpassing the threshold.

Drosophila Lamina neuron physiology

<u>Two-photon imaging</u>

Female flies aged 5-7 days post-eclosion were reared on standard molasses-based food under a 12:12 h light-dark cycle at 25 °C and 60% humidity. Two-photon imaging was performed at room temperature (20 °C). Prior to imaging, flies were cold-anesthetized and mounted onto stainless-steel foil with an opening for the thorax and head. Flies were head-fixed using UV-sensitive glue (Bondic), and their legs were immobilized with bee wax to ensure stability. The head was tilted downward, orienting the fly towards the stimulation screen and exposing the cuticle at the back of the head for dissection. A small window was cut in the cuticle at the back of the head using breakable razor blades. During imaging, the brain was perfused with a carboxygenated saline solution containing: 103 mM NaCl, 3 mM KCl, 5 mM TES, 1 mM NaH_2PO_4, 4 mM $MgCl_2$, 1.5 mM $CaCl_2$, 10 mM trehalose, 10 mM glucose, 7 mM sucrose, and 26 mM $NaHCO_3$. For dissections, the same solution was used without calcium and sugars. The pH of the saline equilibrated near 7.3 when bubbled with 95% O_2 / 5% CO_2. Imaging was performed on a Bruker Ultima microscope equipped with a 20×/NA1.0 objective (Leica, Wetzlar, Germany). Excitation was provided by a fixed-wavelength 930 nm laser (YLMO-930, Menlo Systems, Martinsried, Germany), with 5–15 mW power at the sample. Emitted light passed through a SP680 short-pass filter, a 560 lpxr dichroic mirror, and a 525/70 emission filter. Data were acquired using PrairieView software at ~10 Hz frame rate with an optical zoom of 6×–8×.

783

784 Visual stimulation for two-photon imaging

785 All visual stimuli were generated using custom-written software in PsychoPy[86] and projected onto a
786 9 × 9 cm rear-projection screen placed at a 45° angle in front of the fly, covering 80° of the visual
787 field in both azimuth and elevation. Stimuli were delivered using a LightCrafter projector (Texas
788 Instruments, Dallas, TX, USA) at a frame rate of 100 Hz. The projected light was filtered through a
789 482/18 band-pass filter and a ND1.0 neutral density filter (Thorlabs). The maximum luminance
790 (I_{max}) at the screen was 4.8 μW cm^{-2}.

791

792 Full-field flashes

793 The stimulus consisted of alternating full-field ON (I_{max}) and OFF ($0 \times I_{max}$) flashes, each lasting 5 s.
794 These epochs were repeated at least seven times.

795

796 11_steps_luminance

797 This stimulus consisted of 7 s full-field flashes at 11 luminance levels: 0, 0.1, 0.2, 0.3, 0.4, 0.5, 0.6,
798 0.7, 0.8, 0.9, and $1 \times I_{max}$. Epochs were randomized and repeated at least three times.

799

800 A_B_steps

801 To distinguish contrast-sensitive from luminance-sensitive neurons, we used a stimulus protocol
802 with two consecutive OFF steps (A and B), each lasting 3 s, following a 30 s adapting grey period.
803 The A step consisted of one of six linearly decreasing luminance values, producing six different
804 Weber contrast values relative to the adapting luminance. The subsequent B step also took on one of
805 six decreasing luminance values, selected based on the preceding A step, resulting in six uniform
806 25% Weber contrast steps. A_B epochs were randomized and repeated at least three times.

807

808 Data analysis

809 Data processing was performed using Python 2.7[87]. Pre-processing included motion correction using
810 a Hidden Markov Model from the SIMA Python package[88], followed by manual selection of regions
811 of interest (ROIs). For each imaging frame, the average intensity within each ROI was calculated
812 and background-subtracted to generate time traces. All neural responses and visual stimuli were
813 interpolated to a temporal resolution of 10 Hz. Neural activity was quantified as relative changes in
814 fluorescence over time ($\Delta F/F_0$), where F_0 was defined as the mean fluorescence across the entire
815 trace. Analyses included trial averaging and stimulus-specific evaluations, performed per ROI and
816 then averaged across flies. ROIs showing responses of opposite polarity (i.e., positively correlated
817 with the stimulus), consistent with previous findings[89] were attributed to receptive fields outside the
818 stimulation screen[89]. To exclude these and other noisy ROIs, only those negatively correlated with
819 the stimulus (based on Spearman's rank correlation) and with $\Delta F/F_0$ values exceeding 0.2 were
820 retained.

821

822 Full-field flashes analysis

823 To assess sustained versus transient responses, we calculated the percentage of the peak response
824 retained at the end plateau of the response trace. Peak responses were defined as the difference
825 between the maximum $\Delta F/F_0$ during the stimulus OFF epoch and the mean response 500 ms before
826 stimulus onset. Plateau responses were defined as the difference between the mean $\Delta F/F_0$ during the
827 final 500 ms of the OFF epoch and the same pre-stimulus baseline. The plateau-to-peak ratio was
828 used to characterize response persistence. For the tiny ROIs analysis, multiple small ROIs were

manually drawn for each column, and raw fluorescence traces were extracted and provided for each ROI.

11_steps_luminance analysis

To evaluate luminance encoding, plateau responses were calculated as the mean $\Delta F/F_0$ during the first 500 ms of the final second of each stimulus epoch. These responses were fitted with exponential functions, and the decay rates were quantified. Mutual information between luminance and sustained responses was also computed[90].

A_B_steps analysis

Peak responses were defined as the maximum $\Delta F/F_0$ during each B step, relative to the mean baseline activity in the final 2 s of the adaptation period. Sustained plateau responses were calculated as the mean $\Delta F/F_0$ during the last 500 ms of each step. Luminance dependence was assessed by fitting linear regression models to the responses as a function of luminance, and the resulting slopes were used to quantify the sensitivity.

Statistics

For all *Drosophila* lamina neuron physiology analyses, means were first computed across ROIs within each fly, and then across flies. Statistical comparisons were performed at the fly level. For normally distributed datasets, two-tailed unpaired Student's t-tests were used. Normality was assessed using both the Shapiro-Wilk test ($p>0.05$) and the Kolmogorov-Smirnov test ($p>0.05$). For non-normally distributed data, the Mann-Whitney U test (Wilcoxon rank-sum) was applied.

Mouse tissue preparation

Mice were harvested at postnatal day 18 (P18), and retinas were prepared for analysis as previously described (West et al.[91]). Briefly, retinas were dissected in PBS and fixed for 30 minutes in 4% paraformaldehyde (v/v) with 0.25% Triton-X100 (v/v). After fixation, retinas were washed twice for 5 minutes with 1x PBS, transferred to 7% sucrose in PBS (w/v) for 10 min, and transferred to a 1:1 (v/v) mixture of 30% sucrose in PBS and OCT for 1 hour. Retinas were then frozen in cryomolds and stored at −80 °C.

Mouse HCR-FISH probe design

cDNA for the target transcript was retrieved from Ensembl[78] and partitioned into contiguous 52-nt candidate tiles. Each tile was screened for potential off-targets using NCBI BLAST[92]. The 20 tiles with the fewest predicted off-targets were selected as probe templates. For each selected tile, we generated split-initiator probes by bisecting the tile and appending the appropriate HCR initiator sequence (corresponding to the chosen hairpin amplifier) to each half. Oligonucleotides were synthesized by Integrated DNA Technologies (IDT).

Mouse HCR-FISH

We followed HCR v3.0 protocol from Molecular Instruments[93] with minor modifications. Following dissection and cryosectioning, tissue sections were rinsed twice in PBS to ensure complete thawing. Samples were incubated in pre-warmed PHB for ≥10 min at 37 °C, which was then replaced with

custom-designed probes diluted in PHB (1 µl stock probe solution per 250 µl of buffer) and incubated at 37 °C O/N.

The next day, samples were washed four times for 15 min each with pre-warmed PWB and 5x SSCT with the following ratios: 75% PWB : 25% 5x SSCT, 50:50, 25:75, 0:100. During washes, HCR Amplifiers were heat-activated in a thermal cycler (90 s at 95 °C), and then kept in the dark for 30 min at RT. Samples were washed once with 5x SSCT for 5 min at RT, followed by incubation in AB for ≥30 mins at RT. After cooling, the HCR Amplifiers were diluted in AB (2 ul of 3 uM amplifier stock per 100ul of buffer), added to the samples, and incubated at RT O/N.

The following day, the samples were washed twice for 30 min each in 5x SSCT: first with 100x 405-Wheat Germ Agglutinin, then without. A final wash in 5x SSCT for 5 min was performed before transferring samples to PBS for storage at 4 °C.

QUANTIFICATION AND STATISTICAL ANALYSIS

The number of L3 neurites per cartridge was evaluated by a permutation test (10,000 permutations). All other image-quantification analyses (except *Drosophila* lamina neuron physiology) were performed in Microsoft Excel and GraphPad Prism version 10.5.0[77]. Group comparisons used unpaired t-test, unless otherwise noted. Data are presented as mean ± SEM. Statistical significance was defined as $p < 0.05$, with the following notation: *$p<0.05$, **$p<0.01$, ***$p<0.001$, ns = not significant. All other relevant statistical information can be found in the figure legends.

Drosophila lamina neuron physiology ROI data were averaged per fly before group comparisons. Normality was assessed with Shapiro-Wilk ($p>0.05$) and Kolmogorov-Smirnov ($p>0.05$) tests; normally distributed data were analyzed with unpaired two-tailed t-tests, and non-normally distributed data with the Mann-Whitney U test. *$p<0.05$, **$p<0.01$, ***$p<0.001$, ns = not significant.

SUPPLEMENTAL INFORMATION

Table S1. Custom mouse HCR probe sets and their sequences, related to Figure 6.

Movie S1. GCaMP6f calcium responses in L3 neurons of control animals during full-field visual stimulation, related to Figure 4. This movie corresponds to Figure 4B. Frames were acquired at ~10 Hz. Alternating full-field OFF (0 × Imax) and ON (Imax) flashes, each lasting 5 seconds, were delivered with stimulation onset at 0.0 seconds, 10.0 seconds, and so on. Playback speed is real time. Sample age: 5-7 d adult.

Movie S2. GCaMP6f calcium responses in L3 neurons of Dve-KD animals during full-field visual stimulation, related to Figure 4. This movie corresponds to Figure 4B. Frames were acquired at ~10 Hz. Alternating full-field OFF (0 × Imax) and ON (Imax) flashes, each lasting 5

seconds, were delivered with stimulation onset at 0.0 seconds, 10.0 seconds, and so on. Playback speed is real time. Sample age: 5-7 d adult.

Movie S3. GCaMP6f calcium responses in L2 neurons during full-field visual stimulation, related to Figure 4. This movie corresponds to Figure 4B. Frames were acquired at ~10 Hz. Alternating full-field OFF (0 × Imax) and ON (Imax) flashes, each lasting 5 seconds, were delivered with stimulation onset at 0.0 seconds, 10.0 seconds, and so on. Playback speed is real time. Sample age: 5-7 d adult.

REFERENCES

1. Luo, L. Principles of Neurobiology 2nd ed. (CRC Press).

2. Zeisel, A., Hochgerner, H., Lönnerberg, P., Johnsson, A., Memic, F., van der Zwan, J., Häring, M., Braun, E., Borm, L.E., La Manno, G., et al. (2018). Molecular Architecture of the Mouse Nervous System. Cell *174*, 999-1014.e22. https://doi.org/10.1016/j.cell.2018.06.021.

3. Siletti, K., Hodge, R., Mossi Albiach, A., Lee, K.W., Ding, S.-L., Hu, L., Lönnerberg, P., Bakken, T., Casper, T., Clark, M., et al. (2023). Transcriptomic diversity of cell types across the adult human brain. Science *382*, eadd7046. https://doi.org/10.1126/science.add7046.

4. Li, H., Janssens, J., De Waegeneer, M., Kolluru, S.S., Davie, K., Gardeux, V., Saelens, W., David, F.P.A., Brbić, M., Spanier, K., et al. (2022). Fly Cell Atlas: A single-nucleus transcriptomic atlas of the adult fruit fly. Science *375*, eabk2432. https://doi.org/10.1126/science.abk2432.

5. Nickells, R.W. (1996). Retinal Ganglion Cell Death in Glaucoma: The How, the Why, and the Maybe. J. Glaucoma *5*, 345.

6. Dauer, W., and Przedborski, S. (2003). Parkinson's Disease: Mechanisms and Models. Neuron *39*, 889–909. https://doi.org/10.1016/S0896-6273(03)00568-3.

7. Erclik, T., Li, X., Courgeon, M., Bertet, C., Chen, Z., Baumert, R., Ng, J., Koo, C., Arain, U., Behnia, R., et al. (2017). Integration of temporal and spatial patterning generates neural diversity. Nature *541*, 365–370. https://doi.org/10.1038/nature20794.

8. Sen, S.Q., Chanchani, S., Southall, T.D., and Doe, C.Q. (2019). Neuroblast-specific open chromatin allows the temporal transcription factor, Hunchback, to bind neuroblast-specific loci. eLife *8*, e44036. https://doi.org/10.7554/eLife.44036.

9. Doe, C.Q. (2017). Temporal Patterning in the Drosophila CNS. 24.

10. Briscoe, J., Sussel, L., Serup, P., Hartigan-O'Connor, D., Jessell, T.M., Rubenstein, J.L.R., and Ericson, J. (1999). Homeobox gene Nkx2.2 and speci®cation of neuronal identity by graded Sonic hedgehog signalling. *398*, 6.

11. Briscoe, J., Pierani, A., Jessell, T.M., and Ericson, J. (2000). A Homeodomain Protein Code Specifies Progenitor Cell Identity and Neuronal Fate in the Ventral Neural Tube. Cell *101*, 435–445. https://doi.org/10.1016/S0092-8674(00)80853-3.

12. Petridou, E., and Godinho, L. (2022). Cellular and Molecular Determinants of Retinal Cell Fate. Annu. Rev. Vis. Sci. *8*, 79–99. https://doi.org/10.1146/annurev-vision-100820-103154.

13. Brzezinski, J.A., Prasov, L., and Glaser, T. (2012). *Math5* defines the ganglion cell competence state in a subpopulation of retinal progenitor cells exiting the cell cycle. Dev. Biol. *365*, 395–413. https://doi.org/10.1016/j.ydbio.2012.03.006.

14. Baden, T., Berens, P., Franke, K., Román Rosón, M., Bethge, M., and Euler, T. (2016). The functional diversity of retinal ganglion cells in the mouse. Nature *529*, 345–350. https://doi.org/10.1038/nature16468.

15. Apitz, H., and Salecker, I. (2014). A Challenge of Numbers and Diversity: Neurogenesis in the Drosophila Optic Lobe. J. Neurogenet. *28*, 233–249. https://doi.org/10.3109/01677063.2014.922558.

16. Huang, Z., Shilo, B.Z., and Kunes, S. (1998). A retinal axon fascicle uses Spitz, an EGF receptor ligand, to construct a synaptic cartridge in the brain of Drosophila. Cell *95*, 693–703. https://doi.org/10.1016/S0092-8674(00)81639-6.

17. Huang, Z., and Kunes, S. (1996). Hedgehog, Transmitted along Retinal Axons, Triggers Neurogenesis in the Developing Visual Centers of the Drosophila Brain. Cell *86*, 411–422. https://doi.org/10.1016/S0092-8674(00)80114-2.

18. Xu, C., Ramos, T.B., Rogers, E.M., Reiser, M.B., and Doe, C.Q. (2024). Homeodomain proteins hierarchically specify neuronal diversity and synaptic connectivity. eLife *12*, RP90133. https://doi.org/10.7554/eLife.90133.

19. Tan, L., Zhang, K.X., Pecot, M.Y., Nagarkar-Jaiswal, S., Lee, P.-T., Takemura, S., McEwen, J.M., Nern, A., Xu, S., Tadros, W., et al. (2015). Ig Superfamily Ligand and Receptor Pairs Expressed in Synaptic Partners in Drosophila. Cell *163*, 1756–1769. https://doi.org/10.1016/j.cell.2015.11.021.

20. Piñeiro, C., Lopes, C.S., and Casares, F. (2014). A conserved transcriptional network regulates lamina development in the Drosophila visual system. Development *141*, 2838–2847. https://doi.org/10.1242/dev.108670.

21. Yoo, S., Nair, S., Kim, H., Kim, Y., Lee, C., Lee, G., and Park, J.H. (2020). Knock-in mutations of *scarecrow*, a *Drosophila* homolog of mammalian *Nkx2.1*, reveal a novel function required for development of the optic lobe in *Drosophila melanogaster*. Dev. Biol. *461*, 145–159. https://doi.org/10.1016/j.ydbio.2020.02.008.

22. Fisher, Y.E., Leong, J.C.S., Sporar, K., Ketkar, M.D., Gohl, D.M., Clandinin, T.R., and Silies, M. (2015). A Class of Visual Neurons with Wide-Field Properties Is Required for Local Motion Detection. Curr. Biol. *25*, 3178–3189. https://doi.org/10.1016/j.cub.2015.11.018.

23. Joesch, M., Schnell, B., Raghu, S.V., Reiff, D.F., and Borst, A. (2010). ON and OFF pathways in Drosophila motion vision. Nature *468*, 300–304. https://doi.org/10.1038/nature09545.

24. Tuthill, J.C., Nern, A., Holtz, S.L., Rubin, G.M., and Reiser, M.B. (2013). Contributions of the 12 Neuron Classes in the Fly Lamina to Motion Vision. Neuron *79*, 128–140. https://doi.org/10.1016/j.neuron.2013.05.024.

25. Rivera-Alba, M., Vitaladevuni, S.N., Mishchenko, Y., Lu, Z., Takemura, S., Scheffer, L., Meinertzhagen, I.A., Chklovskii, D.B., and de Polavieja, G.G. (2011). Wiring Economy and

Volume Exclusion Determine Neuronal Placement in the Drosophila Brain. Curr. Biol. *21*, 2000–2005. https://doi.org/10.1016/j.cub.2011.10.022.

26. Ketkar, M.D., Gür, B., Molina-Obando, S., Ioannidou, M., Martelli, C., and Silies, M. (2022). First-order visual interneurons distribute distinct contrast and luminance information across ON and OFF pathways to achieve stable behavior. eLife *11*, e74937. https://doi.org/10.7554/eLife.74937.

27. Ketkar, M.D., Shao, S., Gjorgjieva, J., and Silies, M. (2023). Multifaceted luminance gain control beyond photoreceptors in Drosophila. Curr. Biol. *33*, 2632-2645.e6. https://doi.org/10.1016/j.cub.2023.05.024.

28. Ketkar, M.D., Sporar, K., Gür, B., Ramos-Traslosheros, G., Seifert, M., and Silies, M. (2020). Luminance Information Is Required for the Accurate Estimation of Contrast in Rapidly Changing Visual Contexts. Curr. Biol. *30*, 657-669.e4. https://doi.org/10.1016/j.cub.2019.12.038.

29. Jensen, A.M., and Wallace, V.A. (1997). Expression of Sonic hedgehog and its putative role as a precursor cell mitogen in the developing mouse retina. Development *124*, 363–371. https://doi.org/10.1242/dev.124.2.363.

30. Levine, E.M., Roelink, H., Turner, J., and Reh, T.A. (1997). Sonic Hedgehog Promotes Rod Photoreceptor Differentiation in Mammalian Retinal Cells In Vitro. J. Neurosci. *17*, 6277–6288. https://doi.org/10.1523/JNEUROSCI.17-16-06277.1997.

31. Shekhar, K., Lapan, S.W., Whitney, I.E., Tran, N.M., Macosko, E.Z., Kowalczyk, M., Adiconis, X., Levin, J.Z., Nemesh, J., Goldman, M., et al. (2016). Comprehensive Classification of Retinal Bipolar Neurons by Single-Cell Transcriptomics. Cell *166*, 1308-1323.e30. https://doi.org/10.1016/j.cell.2016.07.054.

32. Wei, W., Liu, B., Jiang, H., Jin, K., and Xiang, M. (2019). Requirement of the Mowat-Wilson Syndrome Gene Zeb2 in the Differentiation and Maintenance of Non-photoreceptor Cell Types During Retinal Development. Mol. Neurobiol. *56*, 1719–1736. https://doi.org/10.1007/s12035-018-1186-6.

33. Wu, F., Kaczynski, T.J., Sethuramanujam, S., Li, R., Jain, V., Slaughter, M., and Mu, X. (2015). Two transcription factors, Pou4f2 and Isl1, are sufficient to specify the retinal ganglion cell fate. Proc. Natl. Acad. Sci. *112*. https://doi.org/10.1073/pnas.1421535112.

34. West, E.R., Lapan, S.W., Lee, C., Kajderowicz, K.M., Li, X., and Cepko, C.L. (2022). Spatiotemporal patterns of neuronal subtype genesis suggest hierarchical development of retinal diversity. Cell Rep. *38*, 110191. https://doi.org/10.1016/j.celrep.2021.110191.

35. Dong, X., Yang, H., Zhou, X., Xie, X., Yu, D., Guo, L., Xu, M., Zhang, W., Liang, G., and Gan, L. (2020). LIM-Homeodomain Transcription Factor LHX4 Is Required for the Differentiation of Retinal Rod Bipolar Cells and OFF-Cone Bipolar Subtypes. Cell Rep. *32*. https://doi.org/10.1016/j.celrep.2020.108144.

36. Balasubramanian, R., Bui, A., Ding, Q., and Gan, L. (2014). Expression of LIM-homeodomain transcription factors in the developing and mature mouse retina. Gene Expr. Patterns *14*, 1–8. https://doi.org/10.1016/j.gep.2013.12.001.

37. Li, J., Choi, J., Cheng, X., Ma, J., Pema, S., Sanes, J.R., Mardon, G., Frankfort, B.J., Tran, N.M., Li, Y., et al. (2024). Comprehensive single-cell atlas of the mouse retina. iScience *27*. https://doi.org/10.1016/j.isci.2024.109916.

38. Bhat, K.M. (1996). The patched signaling pathway mediates repression of gooseberry allowing neuroblast specification by wingless during Drosophila neurogenesis. Dev. Camb. Engl. *122*, 2921–2932. https://doi.org/10.1242/dev.122.9.2921.

39. Chu-LaGraff, Q., and Doe, C.Q. (1993). Neuroblast specification and formation regulated by wingless in the Drosophila CNS. Science *261*, 1594–1597. https://doi.org/10.1126/science.8372355.

40. Doe, C.Q., Fuerstenberg, S., and Peng, C.Y. (1998). Neural stem cells: from fly to vertebrates. J. Neurobiol. *36*, 111–127.

41. McDonald, J.A., and Doe, C.Q. (1997). Establishing neuroblast-specific gene expression in the Drosophila CNS: huckebein is activated by Wingless and Hedgehog and repressed by Engrailed and Gooseberry. Dev. Camb. Engl. *124*, 1079–1087. https://doi.org/10.1242/dev.124.5.1079.

42. Briscoe, J., and Ericson, J. (1999). The specification of neuronal identity by graded Sonic Hedgehog signalling. Semin. Cell Dev. Biol. *10*, 353–362. https://doi.org/10.1006/scdb.1999.0295.

43. Hynes, M., Porter, J.A., Chiang, C., Chang, D., Tessier-Lavigne, M., Beachy, P.A., and Rosenthal, A. (1995). Induction of midbrain dopaminergic neurons by Sonic hedgehog. Neuron *15*, 35–44. https://doi.org/10.1016/0896-6273(95)90062-4.

44. Alenina, N., Bashammakh, S., and Bader, M. (2006). Specification and differentiation of serotonergic neurons. Stem Cell Rev. *2*, 5–10. https://doi.org/10.1007/s12015-006-0002-2.

45. Wang, Y.P., Dakubo, G., Howley, P., Campsall, K.D., Mazarolle, C.J., Shiga, S.A., Lewis, P.M., McMahon, A.P., and Wallace, V.A. (2002). Development of normal retinal organization depends on Sonic hedgehog signaling from ganglion cells. Nat. Neurosci. *5*, 831–832. https://doi.org/10.1038/nn911.

46. Di Bella, D.J., Habibi, E., Stickels, R.R., Scalia, G., Brown, J., Yadollahpour, P., Yang, S.M., Abbate, C., Biancalani, T., Macosko, E.Z., et al. (2021). Molecular logic of cellular diversification in the mouse cerebral cortex. Nature *595*, 554–559. https://doi.org/10.1038/s41586-021-03670-5.

47. Sharma, N., Flaherty, K., Lezgiyeva, K., Wagner, D.E., Klein, A.M., and Ginty, D.D. (2020). The emergence of transcriptional identity in somatosensory neurons. Nature *577*, 392–398. https://doi.org/10.1038/s41586-019-1900-1.

48. Özel, M.N., Simon, F., Jafari, S., Holguera, I., Chen, Y.-C., Benhra, N., El-Danaf, R.N., Kapuralin, K., Malin, J.A., Konstantinides, N., et al. (2021). Neuronal diversity and convergence in a visual system developmental atlas. Nature *589*, 88–95. https://doi.org/10.1038/s41586-020-2879-3.

49. Shekhar, K., Whitney, I.E., Butrus, S., Peng, Y.-R., and Sanes, J.R. (2022). Diversification of multipotential postmitotic mouse retinal ganglion cell precursors into discrete types. eLife *11*, e73809. https://doi.org/10.7554/eLife.73809.

50. Guan, W., Bellemin, S., Bouchet, M., Venkatasubramanian, L., Guillermin, C., Laurençon, A., Kabir, C., Darnas, A., Godin, C., Urdy, S., et al. (2022). Post-transcriptional regulation of transcription factor codes in immature neurons drives neuronal diversity. Cell Rep. *39*. https://doi.org/10.1016/j.celrep.2022.110992.

51. Enriquez, J., Venkatasubramanian, L., Baek, M., Peterson, M., Aghayeva, U., and Mann, R.S. (2015). Specification of Individual Adult Motor Neuron Morphologies by Combinatorial Transcription Factor Codes. Neuron *86*, 955–970. https://doi.org/10.1016/j.neuron.2015.04.011.

52. Hobert, O. (2021). Homeobox genes and the specification of neuronal identity. Nat. Rev. Neurosci. *22*, 627–636. https://doi.org/10.1038/s41583-021-00497-x.

53. Özel, M.N., Gibbs, C.S., Holguera, I., Soliman, M., Bonneau, R., and Desplan, C. (2022). Coordinated control of neuronal differentiation and wiring by sustained transcription factors. Science *378*, eadd1884. https://doi.org/10.1126/science.add1884.

54. Serrano-Saiz, E., Leyva-Díaz, E., De La Cruz, E., and Hobert, O. (2018). BRN3-type POU Homeobox Genes Maintain the Identity of Mature Postmitotic Neurons in Nematodes and Mice. Curr. Biol. *28*, 2813-2823.e2. https://doi.org/10.1016/j.cub.2018.06.045.

55. Skeath, J.B., and Doe, C.Q. (1998). Sanpodo and Notch act in opposition to Numb to distinguish sibling neuron fates in the Drosophila CNS. Dev. Camb. Engl. *125*, 1857–1865. https://doi.org/10.1242/dev.125.10.1857.

56. Mark, B., Lai, S.-L., Zarin, A.A., Manning, L., Pollington, H.Q., Litwin-Kumar, A., Cardona, A., Truman, J.W., and Doe, C.Q. (2021). A developmental framework linking neurogenesis and circuit formation in the Drosophila CNS. eLife *10*, e67510. https://doi.org/10.7554/eLife.67510.

57. Kimble, J., and Simpson, P. (1997). The LIN-12/Notch signaling pathway and its regulation. Annu. Rev. Cell Dev. Biol. *13*, 333–361. https://doi.org/10.1146/annurev.cellbio.13.1.333.

58. Xu, C., Ramos, T.B., Marshall, O.J., and Doe, C.Q. (2024). Notch signaling and Bsh homeodomain activity are integrated to diversify Drosophila lamina neuron types. eLife *12*, RP90136. https://doi.org/10.7554/eLife.90136.

59. Lyons, D.B., and Lomvardas, S. (2014). Repressive histone methylation: a case study in deterministic versus stochastic gene regulation. Biochim. Biophys. Acta *1839*, 1373–1384. https://doi.org/10.1016/j.bbagrm.2014.05.010.

1104 60. Bantignies, F., Roure, V., Comet, I., Leblanc, B., Schuettengruber, B., Bonnet, J., Tixier, V.,
1105 Mas, A., and Cavalli, G. (2011). Polycomb-Dependent Regulatory Contacts between Distant Hox
1106 Loci in Drosophila. Cell *144*, 214–226. https://doi.org/10.1016/j.cell.2010.12.026.

1107 61. Monahan, K., Horta, A., and Lomvardas, S. (2019). LHX2- and LDB1-mediated trans
1108 interactions regulate olfactory receptor choice. Nature *565*, 448–453.
1109 https://doi.org/10.1038/s41586-018-0845-0.

1110 62. Epiney, D.G., Chaya, G.M., Dillon, N.R., Lai, S.-L., and Doe, C.Q. (2025). Single nuclei RNA-
1111 sequencing of adult brain neurons derived from type 2 neuroblasts reveals transcriptional
1112 complexity in the insect central complex. eLife *14*, RP105896.
1113 https://doi.org/10.7554/eLife.105896.

1114 63. Sugino, K., Clark, E., Schulmann, A., Shima, Y., Wang, L., Hunt, D.L., Hooks, B.M., Tränkner,
1115 D., Chandrashekar, J., Picard, S., et al. (2019). Mapping the transcriptional diversity of
1116 genetically and anatomically defined cell populations in the mouse brain. eLife *8*, e38619.
1117 https://doi.org/10.7554/eLife.38619.

1118 64. Reilly, M.B., Cros, C., Varol, E., Yemini, E., and Hobert, O. (2020). Unique homeobox codes
1119 delineate all the neuron classes of C. elegans. Nature *584*, 595–601.
1120 https://doi.org/10.1038/s41586-020-2618-9.

1121 65. Noro, B., Culi, J., McKay, D.J., Zhang, W., and Mann, R.S. (2006). Distinct functions of
1122 homeodomain-containing and homeodomain-less isoforms encoded by homothorax. Genes Dev.
1123 *20*, 1636–1650. https://doi.org/10.1101/gad.1412606.

1124 66. Hasegawa, E., Kaido, M., Takayama, R., and Sato, M. (2013). Brain-specific-homeobox is
1125 required for the specification of neuronal types in the *Drosophila* optic lobe. Dev. Biol. *377*, 90–
1126 99. https://doi.org/10.1016/j.ydbio.2013.02.012.

1127 67. Tian, X., Hansen, D., Schedl, T., and Skeath, J.B. (2004). Epsin potentiates Notch pathway
1128 activity in Drosophila and C. elegans. Dev. Camb. Engl. *131*, 5807–5815.
1129 https://doi.org/10.1242/dev.01459.

1130 68. Johnston, R.J., Otake, Y., Sood, P., Vogt, N., Behnia, R., Vasiliauskas, D., McDonald, E., Xie,
1131 B., Koenig, S., Wolf, R., et al. (2011). Interlocked Feedforward Loops Control Cell-Type-Specific
1132 Rhodopsin Expression in the Drosophila Eye. Cell *145*, 956–968.
1133 https://doi.org/10.1016/j.cell.2011.05.003.

1134 69. Santiago, I.J., Zhang, D., Saras, A., Pontillo, N., Xu, C., Chen, X., Weirauch, M.T., Mistry, M.,
1135 Ginty, D.D., Pecot, M.Y., et al. (2021). Drosophila Fezf functions as a transcriptional repressor to
1136 direct layer-specific synaptic connectivity in the fly visual system. Proc. Natl. Acad. Sci. *118*.
1137 https://doi.org/10.1073/pnas.2025530118.

1138 70. Chen, C.-K., Chen, W.-Y., and Chien, C.-T. (2012). The POU-domain protein Pdm3 regulates
1139 axonal targeting of R neurons in the Drosophila ellipsoid body. Dev. Neurobiol. *72*, 1422–1432.
1140 https://doi.org/10.1002/dneu.22003.

71. Tran, K.D., Miller, M.R., and Doe, C.Q. (2010). Recombineering Hunchback identifies two conserved domains required to maintain neuroblast competence and specify early-born neuronal identity. Development *137*, 1421–1430. https://doi.org/10.1242/dev.048678.

72. Pecot, M.Y., Tadros, W., Nern, A., Bader, M., Chen, Y., and Zipursky, S.L. (2013). Multiple Interactions Control Synaptic Layer Specificity in the Drosophila Visual System. Neuron *77*, 299–310. https://doi.org/10.1016/j.neuron.2012.11.007.

73. Schindelin, J., Arganda-Carreras, I., Frise, E., Kaynig, V., Longair, M., Pietzsch, T., Preibisch, S., Rueden, C., Saalfeld, S., Schmid, B., et al. (2012). Fiji: an open-source platform for biological-image analysis. Nat. Methods *9*, 676–682. https://doi.org/10.1038/nmeth.2019.

74. Schindelin, J., Arganda-Carreras, I., Frise, E., Kaynig, V., Longair, M., Pietzsch, T., Preibisch, S., Rueden, C., Saalfeld, S., Schmid, B., et al. (2012). Fiji: an open-source platform for biological-image analysis. Nat. Methods *9*, 676–682. https://doi.org/10.1038/nmeth.2019.

75. Tarashansky, A.J., Xue, Y., Li, P., Quake, S.R., and Wang, B. (2019). Self-assembling manifolds in single-cell RNA sequencing data. eLife *8*, e48994. https://doi.org/10.7554/eLife.48994.

76. Wolf, F.A., Angerer, P., and Theis, F.J. (2018). SCANPY: large-scale single-cell gene expression data analysis. Genome Biol. *19*, 15. https://doi.org/10.1186/s13059-017-1382-0.

77. Home - GraphPad https://www.graphpad.com/.

78. Dyer, S.C., Austine-Orimoloye, O., Azov, A.G., Barba, M., Barnes, I., Barrera-Enriquez, V.P., Becker, A., Bennett, R., Beracochea, M., Berry, A., et al. (2025). Ensembl 2025. Nucleic Acids Res. *53*, D948–D957. https://doi.org/10.1093/nar/gkae1071.

79. Dombrovski, M., Zang, Y., Frighetto, G., Vaccari, A., Jang, H., Mirshahidi, P.S., Xie, F., Sanfilippo, P., Hina, B.W., Rehan, A., et al. (2025). Molecular gradients shape synaptic specificity of a visuomotor transformation. Nature, 1–10. https://doi.org/10.1038/s41586-025-09037-4.

80. Peng, J., Santiago, I.J., Ahn, C., Gur, B., Tsui, C.K., Su, Z., Xu, C., Karakhanyan, A., Silies, M., and Pecot, M.Y. Drosophila Fezf coordinates laminar-specific connectivity through cell-intrinsic and cell-extrinsic mechanisms. eLife *7*, e33962. https://doi.org/10.7554/eLife.33962.

81. Traag, V.A., Waltman, L., and van Eck, N.J. (2019). From Louvain to Leiden: guaranteeing well-connected communities. Sci. Rep. *9*, 5233. https://doi.org/10.1038/s41598-019-41695-z.

82. Shekhar, K., Lapan, S.W., Whitney, I.E., Tran, N.M., Macosko, E.Z., Kowalczyk, M., Adiconis, X., Levin, J.Z., Nemesh, J., Goldman, M., et al. (2016). Comprehensive Classification of Retinal Bipolar Neurons by Single-Cell Transcriptomics. Cell *166*, 1308-1323.e30. https://doi.org/10.1016/j.cell.2016.07.054.

83. Letunic, I., Doerks, T., and Bork, P. (2015). SMART: recent updates, new developments and status in 2015. Nucleic Acids Res. *43*, D257–D260. https://doi.org/10.1093/nar/gku949.

84. Mi, H., Lazareva-Ulitsky, B., Loo, R., Kejariwal, A., Vandergriff, J., Rabkin, S., Guo, N., Muruganujan, A., Doremieux, O., Campbell, M.J., et al. (2005). The PANTHER database of protein families, subfamilies, functions and pathways. Nucleic Acids Res. *33*, D284–D288. https://doi.org/10.1093/nar/gki078.

85. Smedley, D., Haider, S., Ballester, B., Holland, R., London, D., Thorisson, G., and Kasprzyk, A. (2009). BioMart – biological queries made easy. BMC Genomics *10*, 22. https://doi.org/10.1186/1471-2164-10-22.

86. Peirce, J.W. (2008). Generating Stimuli for Neuroscience Using PsychoPy. Front. Neuroinformatics *2*, 10. https://doi.org/10.3389/neuro.11.010.2008.

87. van Rossum, G. (1995). Python reference manual.

88. Kaifosh, P., Zaremba, J.D., Danielson, N.B., and Losonczy, A. (2014). SIMA: Python software for analysis of dynamic fluorescence imaging data. Front. Neuroinformatics *8*, 80. https://doi.org/10.3389/fninf.2014.00080.

89. Fisher, Y.E., Leong, J.C.S., Sporar, K., Ketkar, M.D., Gohl, D.M., Clandinin, T.R., and Silies, M. (2015). A Class of Visual Neurons with Wide-Field Properties Is Required for Local Motion Detection. Curr. Biol. CB *25*, 3178–3189. https://doi.org/10.1016/j.cub.2015.11.018.

90. Ross, B.C. (2014). Mutual information between discrete and continuous data sets. PloS One *9*, e87357. https://doi.org/10.1371/journal.pone.0087357.

91. West, E.R., Lapan, S.W., Lee, C., Kajderowicz, K.M., Li, X., and Cepko, C.L. (2022). Spatiotemporal patterns of neuronal subtype genesis suggest hierarchical development of retinal diversity. Cell Rep. *38*. https://doi.org/10.1016/j.celrep.2021.110191.

92. Camacho, C., Coulouris, G., Avagyan, V., Ma, N., Papadopoulos, J., Bealer, K., and Madden, T.L. (2009). BLAST+: architecture and applications. BMC Bioinformatics *10*, 421. https://doi.org/10.1186/1471-2105-10-421.

93. Choi, H.M.T., Schwarzkopf, M., Fornace, M.E., Acharya, A., Artavanis, G., Stegmaier, J., Cunha, A., and Pierce, N.A. (2018). Third-generation in situ hybridization chain reaction: multiplexed, quantitative, sensitive, versatile, robust. Development *145*, dev165753. https://doi.org/10.1242/dev.165753.

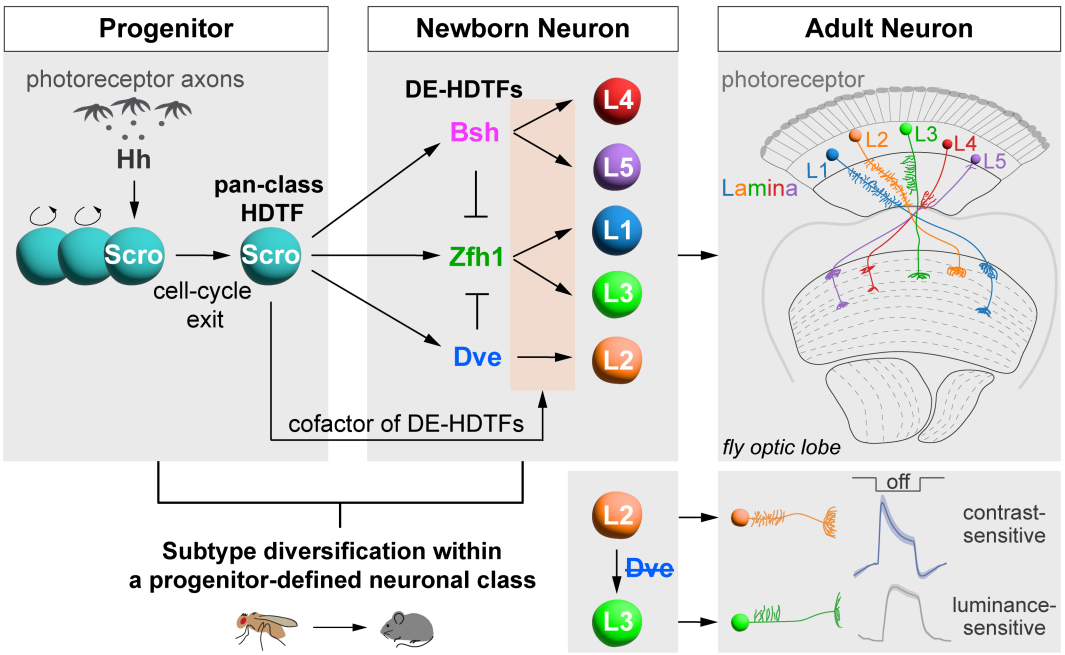

Graphical abstract

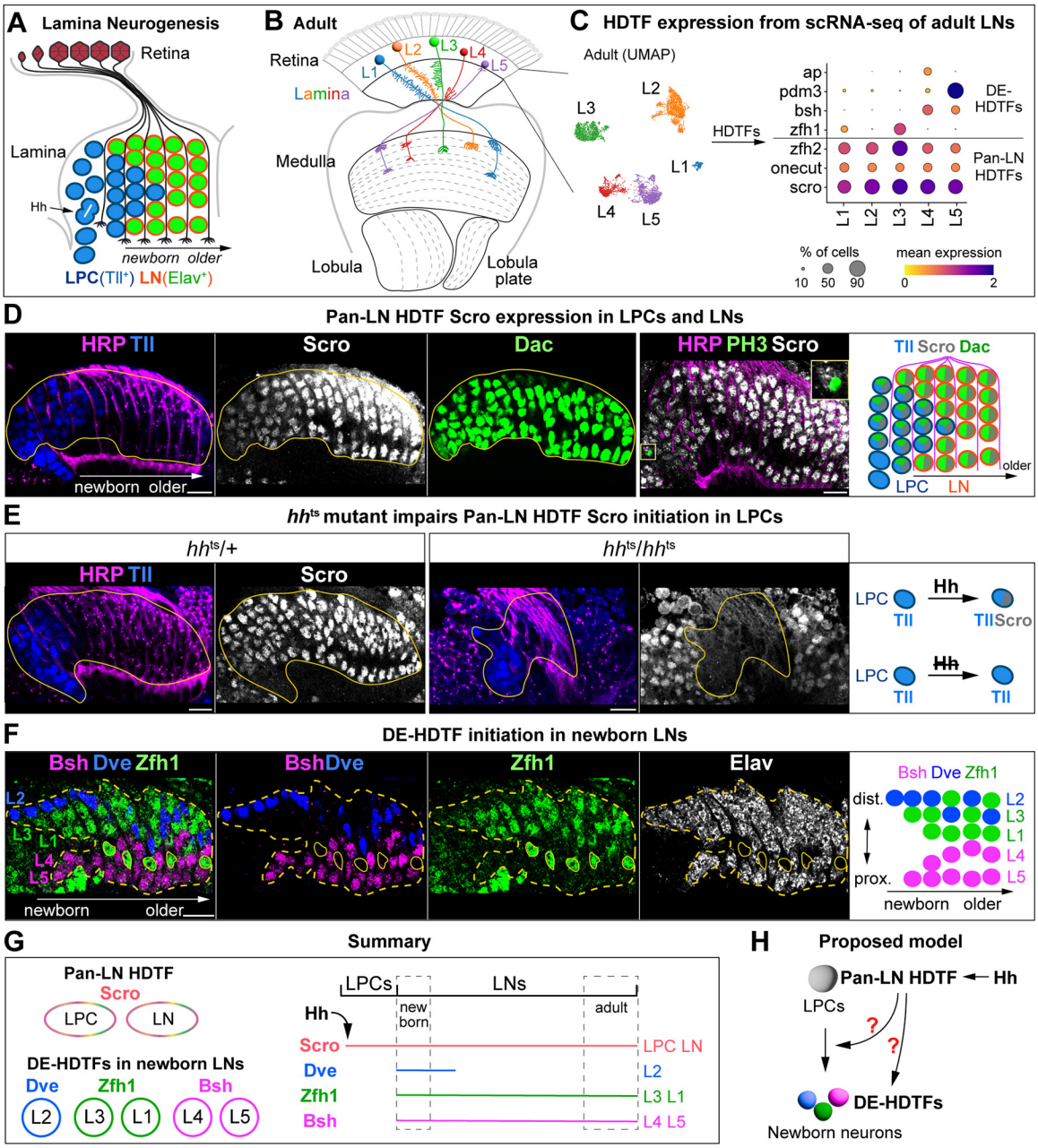
A Lamina Neurogenesis
Retina
Lamina
Hh
newborn older
LPC(Tll+) LN(Elav+)
B Adult
Retina
Lamina
Medulla
Lobula
Lobula plate
L1 L2 L3 L4 L5
C HDTF expression from scRNA-seq of adult LNs
Adult (UMAP)
L3 L2 L1 L4 L5
HDTFs
ap
pdm3
bsh
zfh1
zfh2
onecut
scro
DE-HDTFs
Pan-LN HDTFs
% of cells
10 50 90
mean expression
0 2
D Pan-LN HDTF Scro expression in LPCs and LNs
HRP Tll
Scro
Dac
HRP PH3 Scro
Tll Scro Dac
newborn older
LPC LN
E hhts mutant impairs Pan-LN HDTF Scro initiation in LPCs
hhts/+
hhts/hhts
HRP Tll
Scro
LPC Tll
Hh
Tll Scro
LPC Tll
Hh
Tll
F DE-HDTF initiation in newborn LNs
Bsh Dve Zfh1
BshDve
Zfh1
Elav
L2 L3 L1 L4 L5
newborn older
Bsh Dve Zfh1
dist.
prox.
L2 L3 L1 L4 L5
newborn older
G Summary
Pan-LN HDTF
Scro
LPC LN
DE-HDTFs in newborn LNs
Dve Zfh1 Bsh
L2 L3 L1 L4 L5
LPCs LNs
Hh
new born
adult
Scro LPC LN
Dve L2
Zfh1 L3 L1
Bsh L4 L5
H Proposed model
Pan-LN HDTF
Hh
LPCs
?
?
DE-HDTFs
Newborn neurons

Figure 1

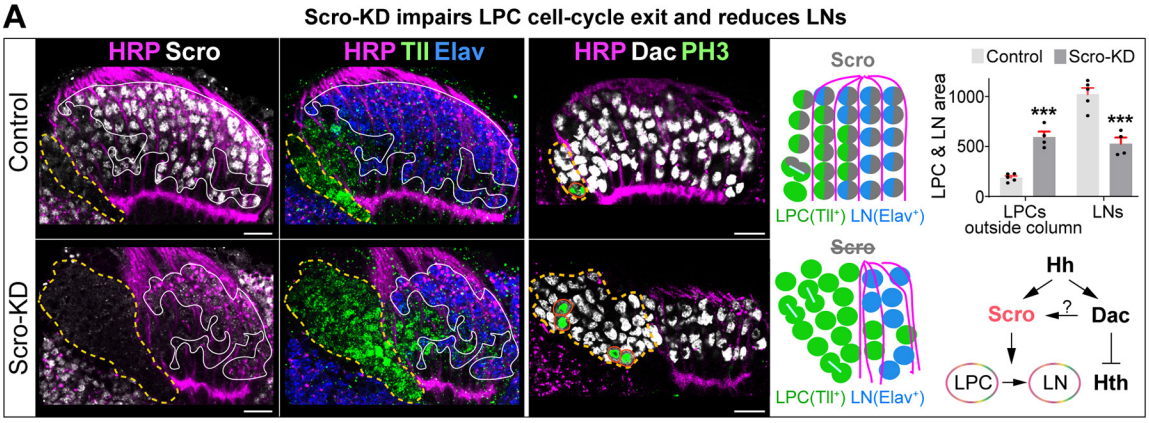
A
Scro-KD impairs LPC cell-cycle exit and reduces LNs
Control
Scro-KD
HRP Scro
HRP Tll Elav
HRP Dac PH3
Scro
LPC(Tll+) LN(Elav+)
Control Scro-KD
LPC & LN area
1000
500
0
***
LPCs outside column
LNs
Hh
Scro
?
Dac
LPC
LN
Hth

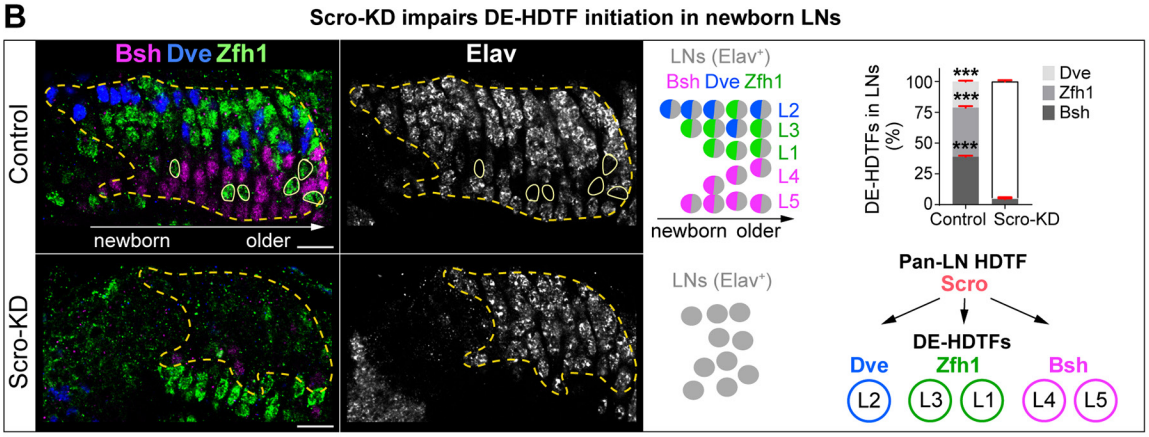
B
Scro-KD impairs DE-HDTF initiation in newborn LNs
Control
Scro-KD
Bsh Dve Zfh1
Elav
newborn
older
LNs (Elav+)
Bsh Dve Zfh1
L2
L3
L1
L4
L5
DE-HDTFs in LNs (%)
100
75
50
25
0
Control Scro-KD
Dve
Zfh1
Bsh
Pan-LN HDTF
Scro
DE-HDTFs
Dve
Zfh1
Bsh
L2
L3
L1
L4
L5

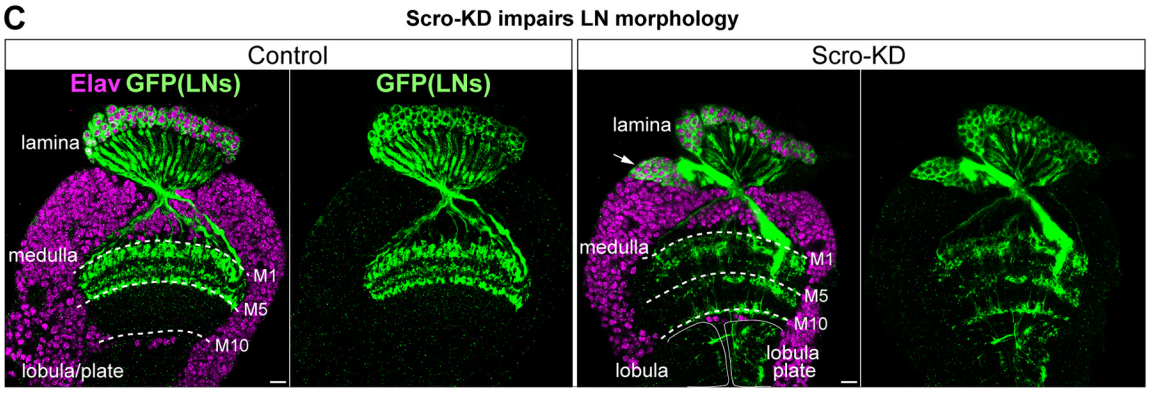
C
Scro-KD impairs LN morphology
Control
Scro-KD
Elav GFP(LNs)
GFP(LNs)
lamina
medulla
M1
M5
M10
lobula/plate
lobula
lobula plate

Figure 2

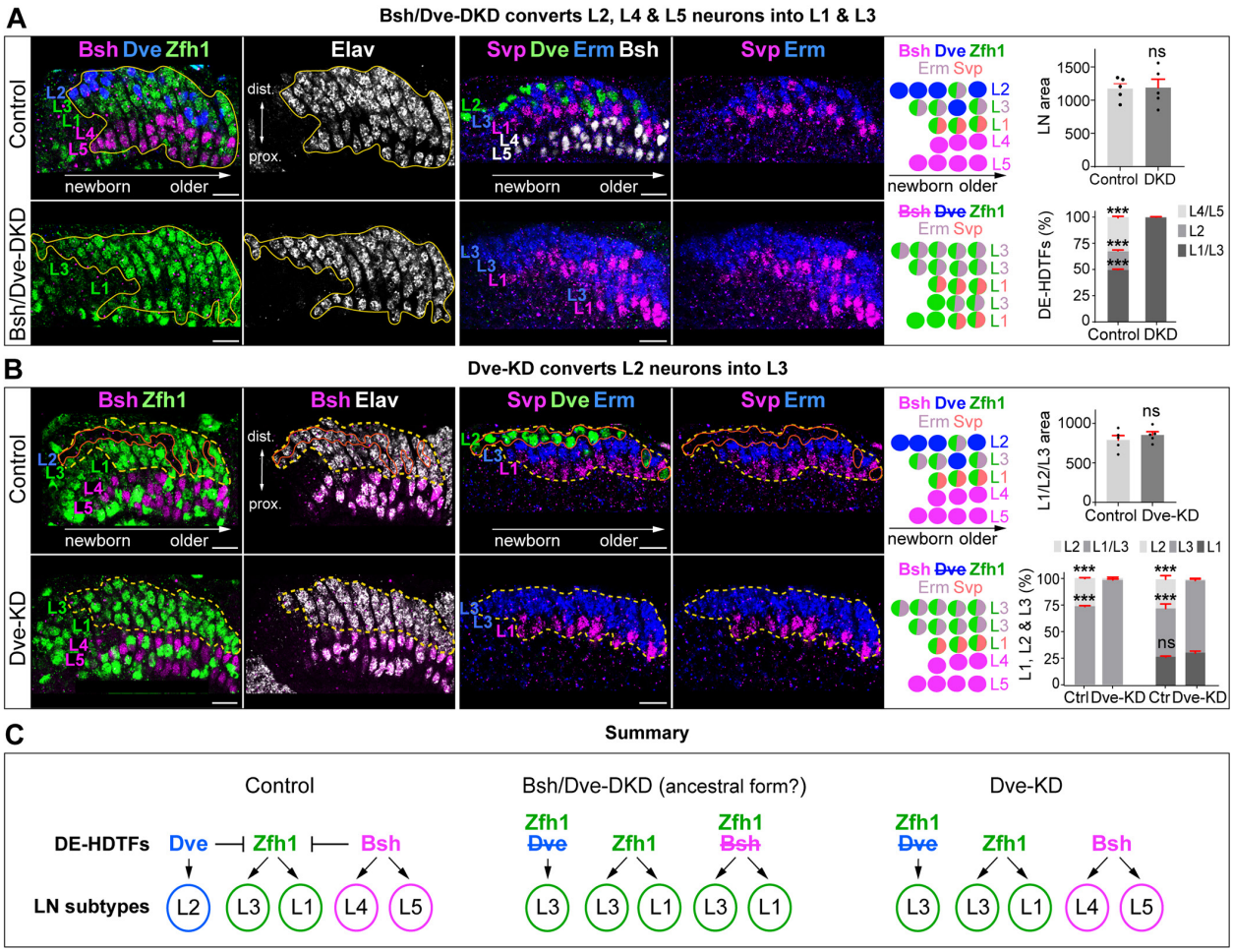
A
Bsh/Dve-DKD converts L2, L4 & L5 neurons into L1 & L3
Control
Bsh/Dve-DKD
Bsh Dve Zfh1
Elav
Svp Dve Erm Bsh
Svp Erm
newborn
older
dist.
prox.
Bsh Dve Zfh1
Erm Svp
newborn older
LN area
ns
Control DKD
DE-HDTFs (%)
L4/L5
L2
L1/L3
B
Dve-KD converts L2 neurons into L3
Dve-KD
Bsh Zfh1
Bsh Elav
Svp Dve Erm
L1/L2/L3 area
Control Dve-KD
L1, L2 & L3 (%)
Ctrl Dve-KD Ctr Dve-KD
C
Summary
Control
Bsh/Dve-DKD (ancestral form?)
Dve-KD
DE-HDTFs
LN subtypes
Dve
Zfh1
Bsh
L2
L3
L1
L4
L5

Figure 3

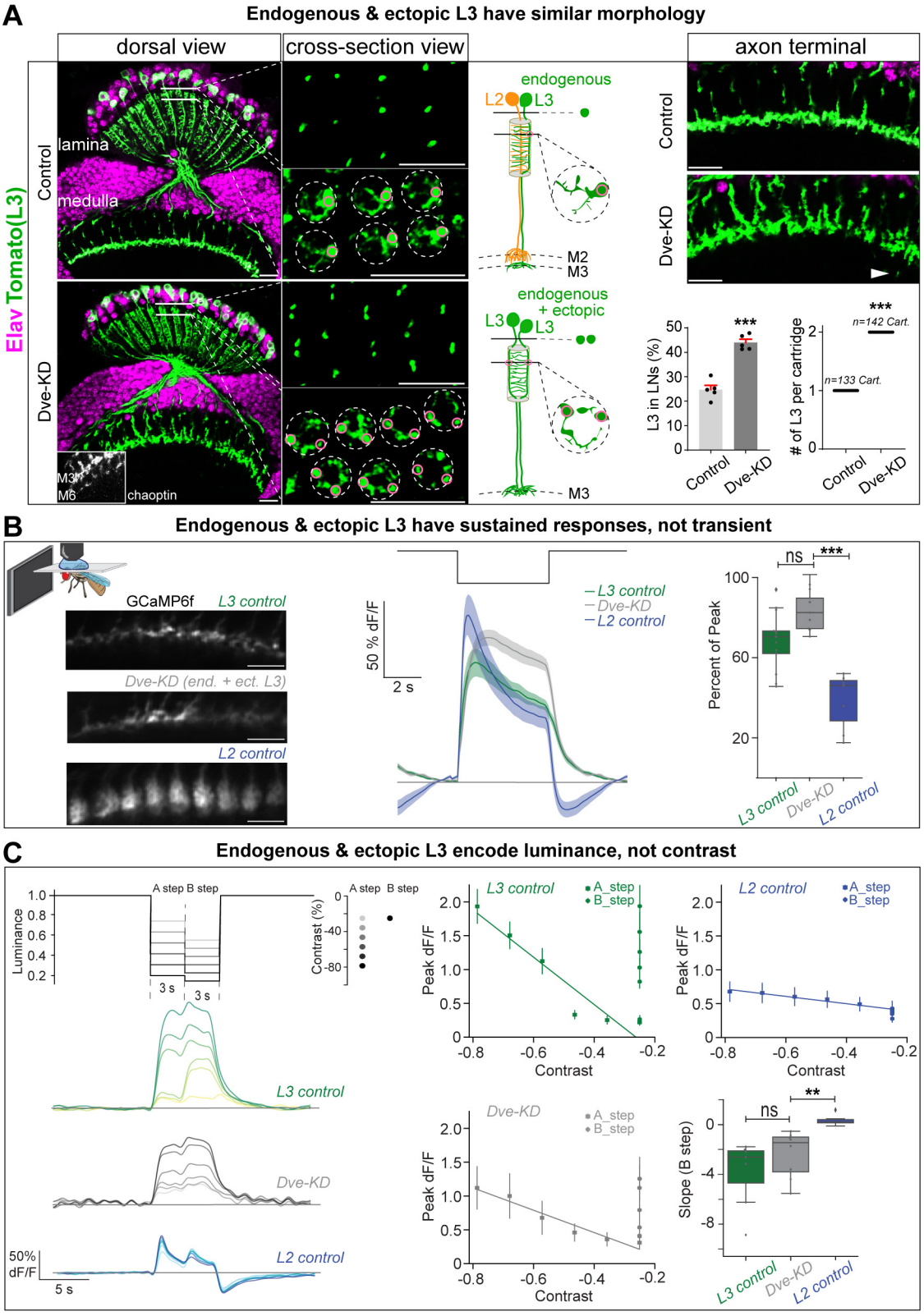
A
Endogenous & ectopic L3 have similar morphology
dorsal view
cross-section view
axon terminal
Elav Tomato(L3)
Control
Dve-KD
lamina
medulla
M3
M6
chaoptin
endogenous
L2
L3
M2
M3
endogenous
+ ectopic
L3
L3
M3
L3 in LNs (%)
***
Control
Dve-KD
# of L3 per cartridge
***
n=142 Cart.
n=133 Cart.
B
Endogenous & ectopic L3 have sustained responses, not transient
GCaMP6f
L3 control
Dve-KD (end. + ect. L3)
L2 control
50 % dF/F
2 s
L3 control
Dve-KD
L2 control
Percent of Peak
ns
***
C
Endogenous & ectopic L3 encode luminance, not contrast
Luminance
A step B step
3 s
3 s
Contrast (%)
L3 control
Dve-KD
L2 control
50% dF/F
5 s
Peak dF/F
Contrast
A_step
B_step
Slope (B step)
ns
**

Figure 4

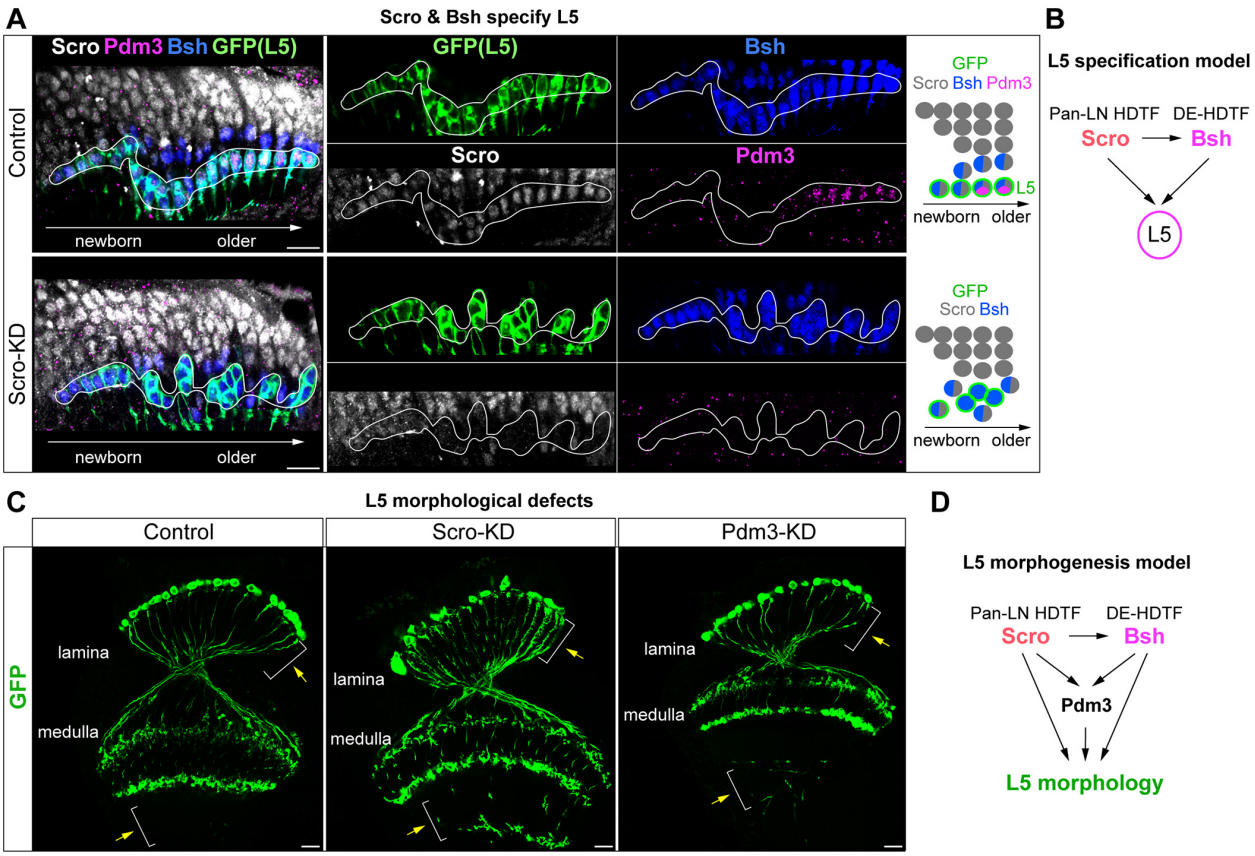
A
Scro & Bsh specify L5
Scro Pdm3 Bsh GFP(L5)
GFP(L5)
Bsh
Scro
Pdm3
Control
Scro-KD
newborn
older
GFP
Scro Bsh Pdm3
L5
Scro Bsh
B
L5 specification model
Pan-LN HDTF
DE-HDTF
Scro
Bsh
L5
C
L5 morphological defects
Control
Scro-KD
Pdm3-KD
GFP
lamina
medulla
D
L5 morphogenesis model
Pan-LN HDTF
DE-HDTF
Scro
Bsh
Pdm3
L5 morphology

Figure 5

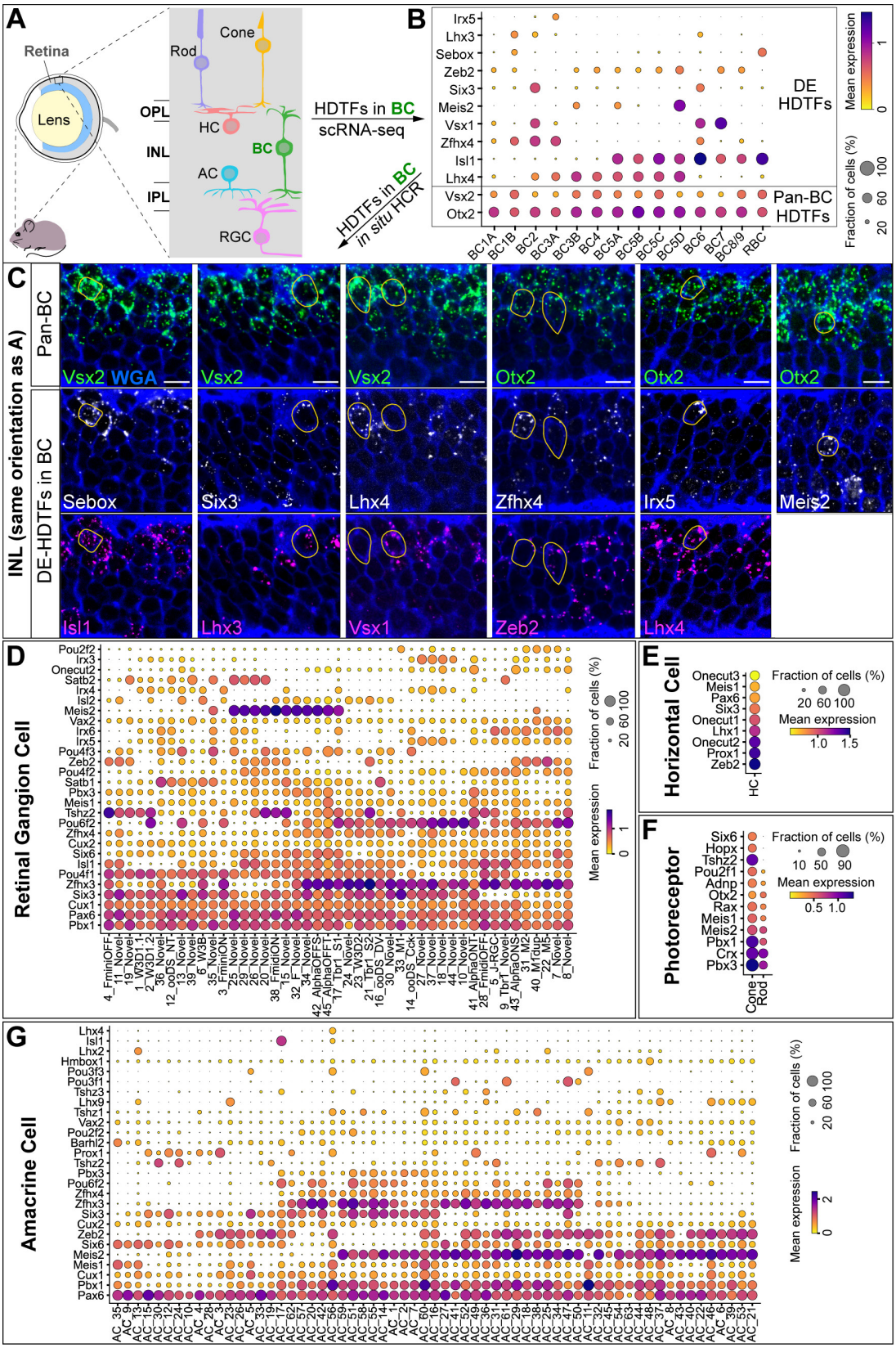
A
Retina
Lens
Rod
Cone
OPL
HC
INL
BC
AC
IPL
RGC
HDTFs in BC
scRNA-seq
HDTFs in BC
in situ HCR
B
Irx5
Lhx3
Sebox
Zeb2
Six3
Meis2
Vsx1
Zfhx4
Isl1
Lhx4
Vsx2
Otx2
DE
HDTFs
Pan-BC
HDTFs
BC1A
BC1B
BC2
BC3A
BC3B
BC4
BC5A
BC5B
BC5C
BC5D
BC6
BC7
BC8/9
RBC
Mean expression
Fraction of cells (%)
C
INL (same orientation as A)
Pan-BC
DE-HDTFs in BC
Vsx2 WGA
Vsx2
Vsx2
Otx2
Otx2
Otx2
Sebox
Six3
Lhx4
Zfhx4
Irx5
Meis2
Isl1
Lhx3
Vsx1
Zeb2
Lhx4
D
Retinal Gangion Cell
Pou2f2
Irx3
Onecut2
Satb2
Irx4
Isl2
Meis2
Vax2
Irx6
Irx5
Pou4f3
Zeb2
Pou4f2
Satb1
Pbx3
Meis1
Tshz2
Pou6f2
Zfhx4
Cux2
Six6
Isl1
Pou4f1
Zfhx3
Six3
Cux1
Pax6
Pbx1
Fraction of cells (%)
Mean expression
E
Horizontal Cell
Onecut3
Meis1
Pax6
Six3
Onecut1
Lhx1
Onecut2
Prox1
Zeb2
HC-1
Fraction of cells (%)
Mean expression
F
Photoreceptor
Six6
Hopx
Tshz2
Pou2f1
Adnp
Otx2
Rax
Meis1
Meis2
Pbx1
Crx
Pbx3
Cone
Rod
Fraction of cells (%)
Mean expression
G
Amacrine Cell
Lhx4
Isl1
Lhx2
Hmbox1
Pou3f3
Pou3f1
Tshz3
Lhx9
Tshz1
Vax2
Pou2f2
Barhl2
Prox1
Tshz2
Pbx3
Pou6f2
Zfhx4
Zfhx3
Six3
Cux2
Zeb2
Six6
Meis2
Meis1
Cux1
Pbx1
Pax6
Fraction of cells (%)
Mean expression

Figure 6

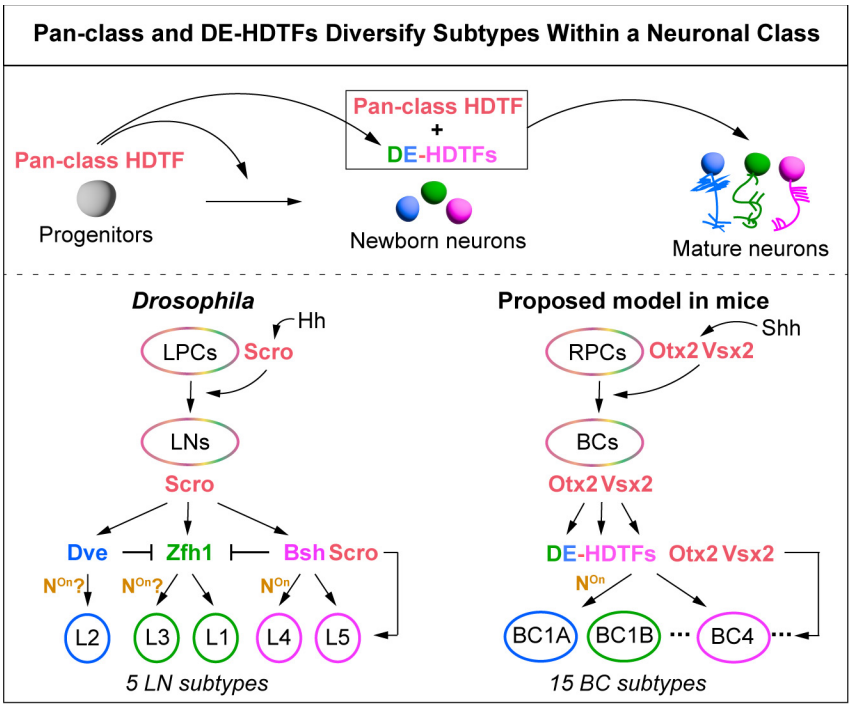
Pan-class and DE-HDTFs Diversify Subtypes Within a Neuronal Class
Pan-class HDTF
Progenitors
Pan-class HDTF
+
DE-HDTFs
Newborn neurons
Mature neurons
Drosophila
Hh
LPCs
Scro
LNs
Scro
Dve
Zfh1
Bsh
Scro
NOn?
NOn?
NOn
L2
L3
L1
L4
L5
5 LN subtypes
Proposed model in mice
Shh
RPCs
Otx2 Vsx2
BCs
Otx2 Vsx2
DE-HDTFs
Otx2 Vsx2
NOn
BC1A
BC1B
BC4
15 BC subtypes

Figure 7

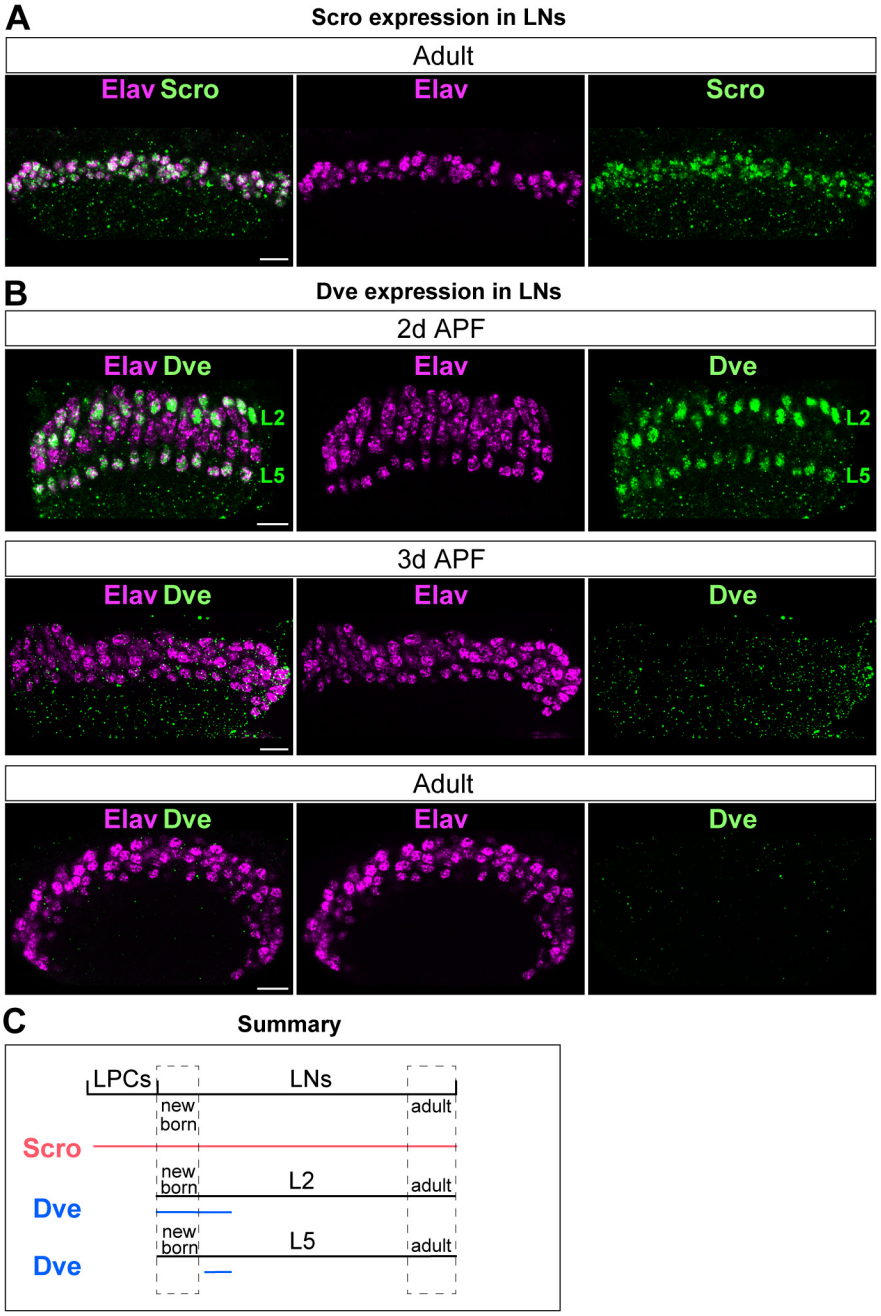
A
Scro expression in LNs
Adult
Elav Scro
Elav
Scro
B
Dve expression in LNs
2d APF
Elav Dve
L2
L5
Elav
Dve
L2
L5
3d APF
Elav Dve
Elav
Dve
Adult
Elav Dve
Elav
Dve
C
Summary
LPCs
LNs
new born
adult
Scro
new born
L2
adult
Dve
new born
L5
adult
Dve

Figure S1

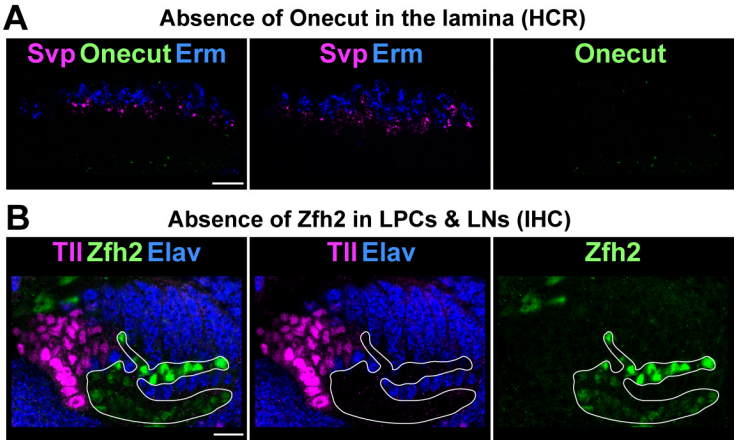
A
Absence of Onecut in the lamina (HCR)
Svp Onecut Erm
Svp Erm
Onecut
B
Absence of Zfh2 in LPCs & LNs (IHC)
Tll Zfh2 Elav
Tll Elav
Zfh2

Figure S2

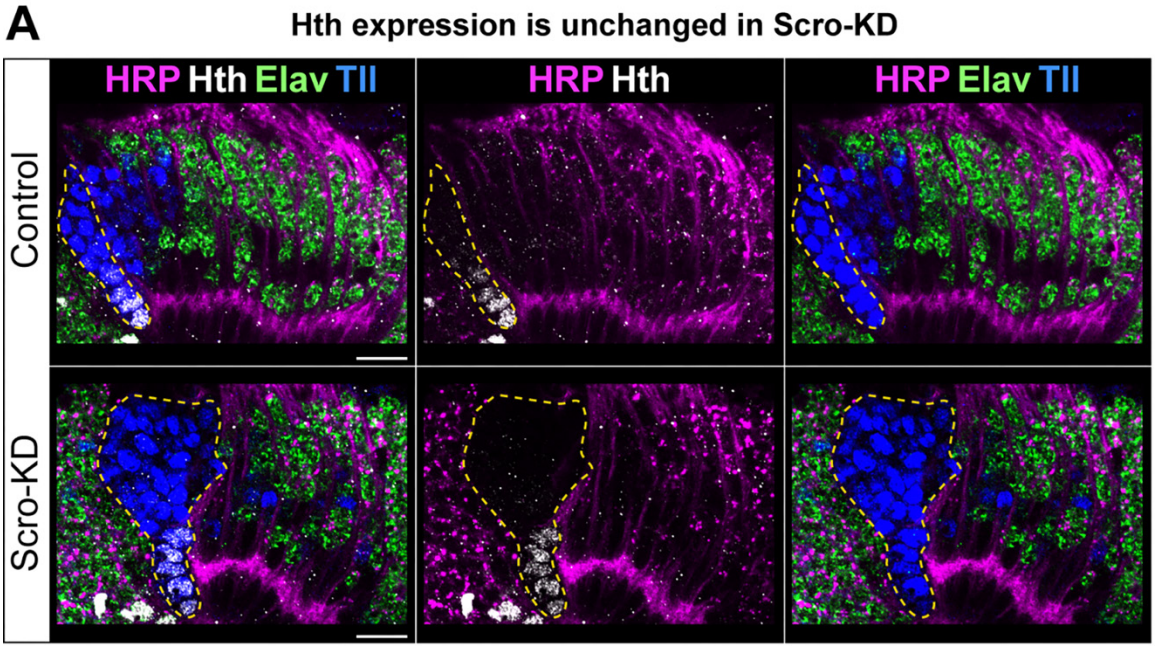
A
Hth expression is unchanged in Scro-KD
HRP Hth Elav Tll
HRP Hth
HRP Elav Tll
Control
Scro-KD

Figure S3

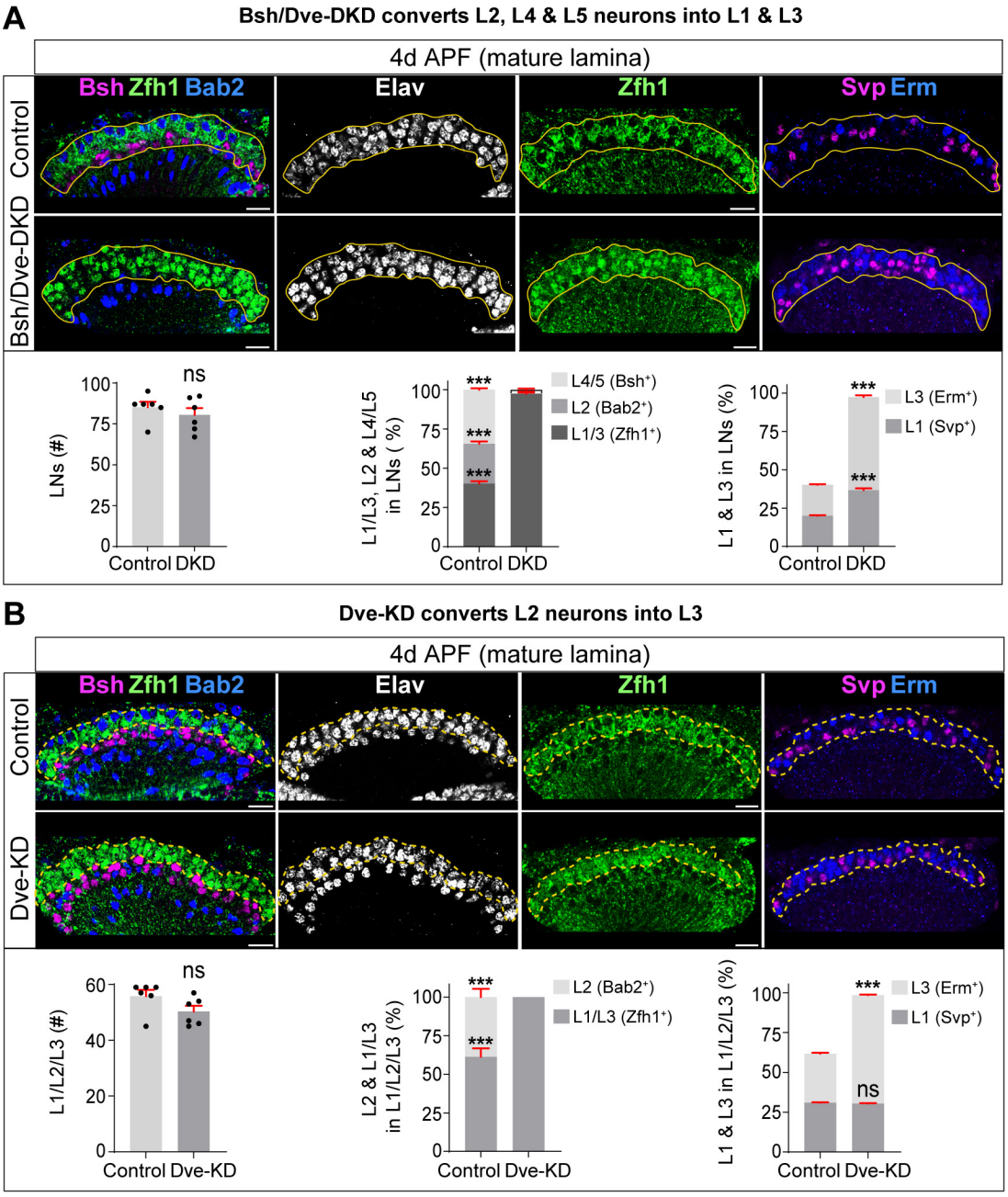
A
Bsh/Dve-DKD converts L2, L4 & L5 neurons into L1 & L3
4d APF (mature lamina)
Bsh Zfh1 Bab2
Elav
Zfh1
Svp Erm
Control
Bsh/Dve-DKD
LNs (#)
ns
Control DKD
L1/L3, L2 & L4/L5 in LNs (%)
L4/5 (Bsh+)
L2 (Bab2+)
L1/3 (Zfh1+)
L1 & L3 in LNs (%)
L3 (Erm+)
L1 (Svp+)
B
Dve-KD converts L2 neurons into L3
4d APF (mature lamina)
Control
Dve-KD
L1/L2/L3 (#)
Control Dve-KD
L2 & L1/L3 in L1/L2/L3 (%)
L2 (Bab2+)
L1/L3 (Zfh1+)
L1 & L3 in L1/L2/L3 (%)
L3 (Erm+)
L1 (Svp+)

Figure S4

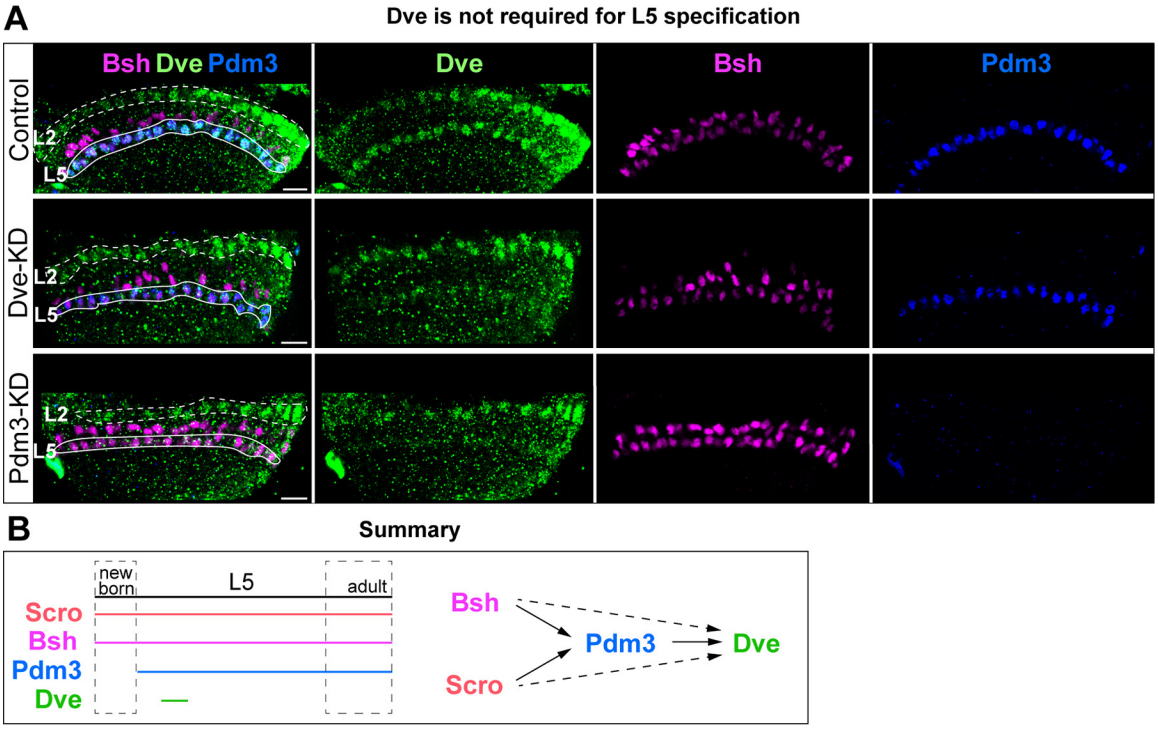
A
Dve is not required for L5 specification
Bsh Dve Pdm3
Dve
Bsh
Pdm3
Control
Dve-KD
Pdm3-KD
L2
L5
B
Summary
new born
L5
adult
Scro
Bsh
Pdm3
Dve
Bsh
Scro
Pdm3
Dve

Figure S5

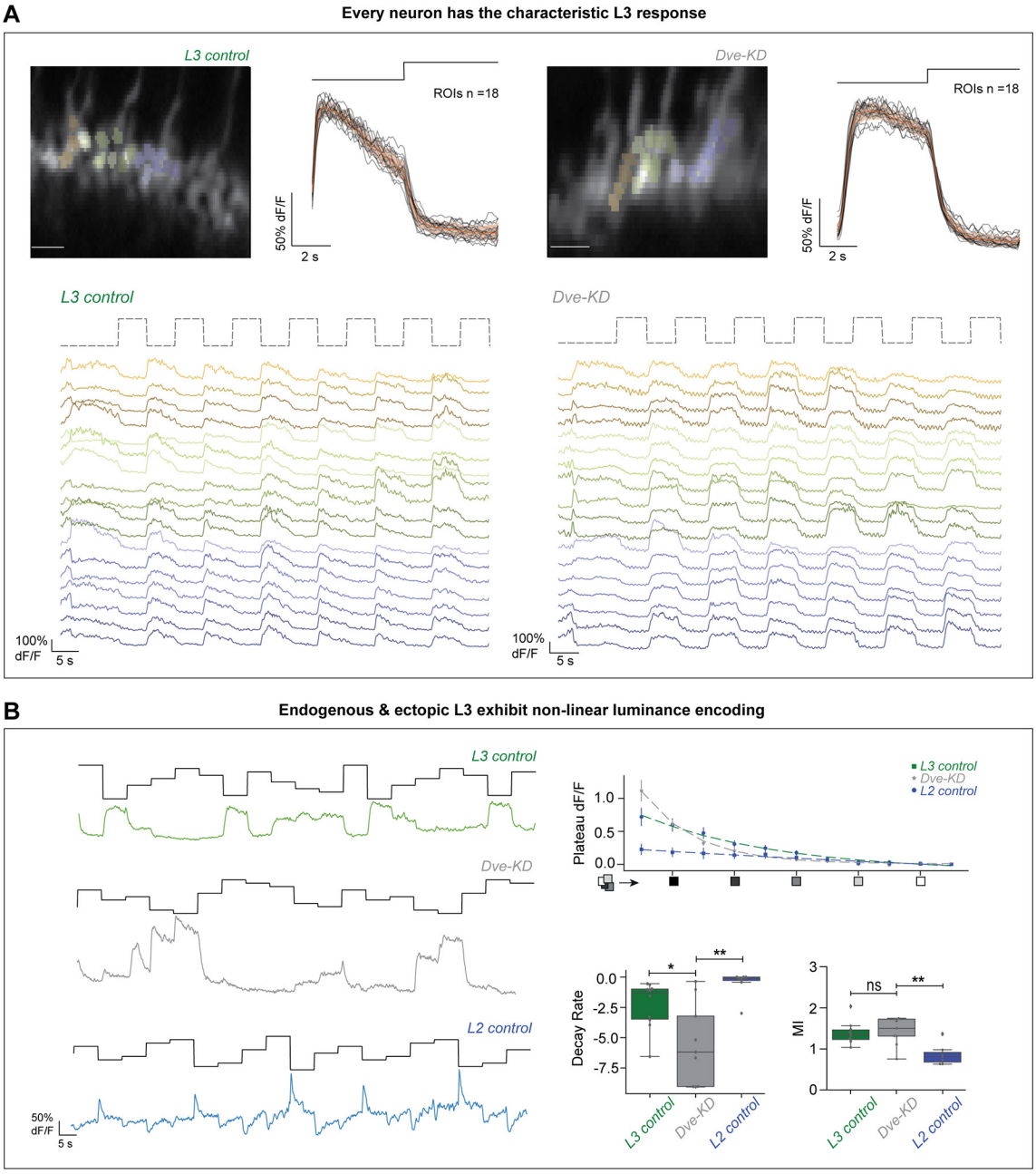
A
Every neuron has the characteristic L3 response
L3 control
ROIs n =18
50% dF/F
2 s
Dve-KD
ROIs n =18
50% dF/F
2 s
L3 control
Dve-KD
100% dF/F
5 s
100% dF/F
5 s
B
Endogenous & ectopic L3 exhibit non-linear luminance encoding
L3 control
Dve-KD
L2 control
50% dF/F
5 s
L3 control
Dve-KD
L2 control
Plateau dF/F
1.0
0.5
0.0
Decay Rate
0.0
-2.5
-5.0
-7.5
*
**
MI
3
2
1
0
ns
**
L3 control
Dve-KD
L2 control

Figure S6

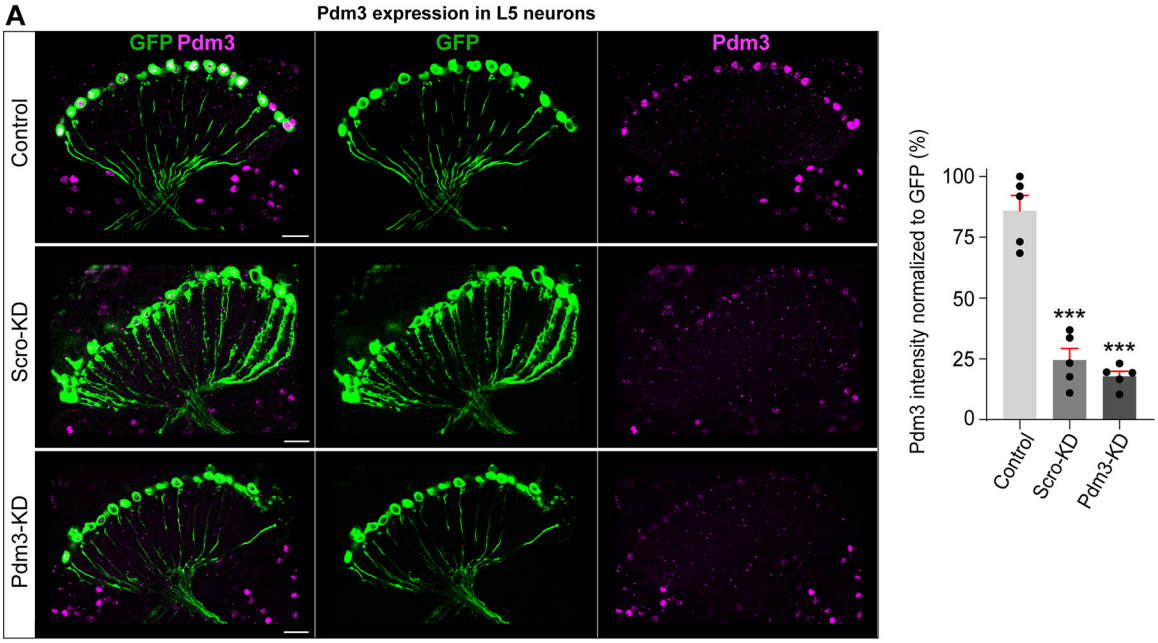
A
Pdm3 expression in L5 neurons
GFP Pdm3
GFP
Pdm3
Control
Scro-KD
Pdm3-KD
Pdm3 intensity normalized to GFP (%)
100
75
50
25
0
***
***
Control
Scro-KD
Pdm3-KD

Figure S7